On the difference between thermalization in open and isolated quantum systems: a case study

Archak Purkayastha[1,*], Giacomo Guarnieri[2], Janet Anders[3,4], Marco Merkli[5]

[1] Department of Physics, Indian Institute of Technology, Hyderabad 502284, India.
[2] Department of Physics A. Volta, University of Pavia, Via Bassi 6, 27100, Pavia, Italy
[3] Physics and Astronomy, University of Exeter, Exeter EX4 4QL, United Kingdom.
[4] Institut für Physik, Potsdam University, 14476 Potsdam, Germany.
[5] Department of Mathematics and Statistics, Memorial University of Newfoundland,
St. John's, NL, Canada A1C 5S7
* archak.p@phy.iith.ac.in

July 23, 2025

Abstract

Thermalization of isolated and open quantum systems has been studied extensively. However, being the subject of investigation by different scientific communities and being analysed using different mathematical tools, the connection between the isolated (IQS) and open (OQS) approaches to thermalization has remained opaque. Here we demonstrate that the fundamental difference between the two paradigms is the order in which the long time and the thermodynamic limits are taken. This difference implies that they describe physics on widely different time and length scales. Our analysis is carried out numerically for the case of a double quantum dot (DQD) coupled to a fermionic lead. We show how both OQS and IQS thermalization can be explored in this model on equal footing, allowing a fair comparison between the two. We find that while the quadratically coupled (free) DQD experiences no isolated thermalization, it of course does experience open thermalization. For the non-linearly interacting DQD coupled to a fermionic lead, the many-body interaction in the DQD breaks the integrability of the whole system. We find that this system shows strong evidence of both OQS and IQS thermalization in the same dynamics, but at widely different time scales, consistent with reversing the order of the long time and the thermodynamic limits.

Contents

1 Introduction

Common experience shows that a system kept in contact with surroundings at a given temperature eventually thermalizes to that temperature. This forms the basis of much of standard thermodynamics and statistical physics. Yet, how such a process can consistently arise from the principles of quantum mechanics has been one of the fundamental questions, with a long history across physics [1–13] and mathematics [14–22]. Two classes of approaches to this problem have now become well-established. The first is the open quantum system (OQS) approach. In this approach, the surrounding environment (bath) of the system is usually modelled via a continuum of bosonic or fermionic modes, initially in a Gibbs state with a given temperature, uncorrelated with the system. Equations describing the dynamics of the system are then derived by formally integrating out the bath degrees of freedom. This can be done in any of the standard approaches to OQS, like quantum master equations [23, 24], non-equilibrium Green's functions, Feynman-Vernon influence functional, Keldysh-Schwinger path integrals [25–27] and quantum Langevin equations [12, 13, 28–32]. The OQS approach then aims to show that, irrespective of the initial state of the system, in the long-time limit, the system approaches a steady state consistent with the initial temperature of the bath. This state of the system is expected to be the marginal of the global Gibbs state of the system and the bath [7–13]. This is the starting point of many strong-coupling approaches to quantum thermodynamics, where such a state is called the mean-force Gibbs state (MGS) [33–35]. To the leading order for a small system-bath coupling, the MGS is the Gibbs state of the system with the temperature of the bath, which is completely consistent with the notion of thermalization in standard statistical physics. Considerable efforts have historically been dedicated to derive physically consistent weak system-bath coupling quantum master equations for the system degrees of freedom, satisfying convergence to the Gibbs state of the system [23]. The fundamental limitations of such an approach have been appreciated only recently [36, 37], and an improved quantum master equation that ensures convergence to the MGS has been derived [38].

In a second well-established approach to describing the process of thermalization, no demarcation is made between the system and the surroundings. The whole set-up is taken to be isolated and evolving according to a global, hermitian Hamiltonian [4, 6, 39–61]. We call this the Isolated Quantum System (IQS) approach. A particularly important view within the IQS approach is the so-called Eigenstate Thermalization Hypothesis (ETH) [1–3, 5, 44, 50], which has become a cornerstone in the present understanding of chaos and integrability in quantum
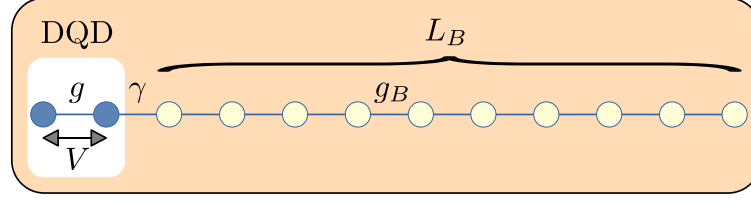
Figure 1: *Schematic of DQD coupled to a fermionic lead.* The system of interest is that of two fermionic sites (blue discs) which form a double quantum dot (DQD). The DQD is linearly coupled to a chain of L_B fermionic sites (yellow discs) that represent a fermionic lead (bath). The hopping (blue lines) within the lead is g_B. The hopping constant within the DQD is g, while between the DQD and the lead it is γ. In addition, a nearest neighbour repulsive many-body interaction with strength V (grey arrow) may act between the two sites of the DQD. The Hamiltonian for the full, closed, spinless fermion chain (orange box) is given by (1). We refer to $V = 0$ as the *free fermion model*, and to $V > 0$ as the *interacting DQD model*.

many-body systems. In the ETH approach, the initial state of the global set-up is taken to be a generic state which is sharply peaked at some given energy, and it is assumed that the global Hamiltonian is non-integrable [50]. It is then argued that for large times, the state of any small subsystem of the entire set-up relaxes to the marginal of the global Gibbs state, up to sub-extensive corrections. The temperature of the Gibbs state is consistent with the energy of the global state.

The non-integrability condition is not fulfilled for 'free' models, for which the Hamiltonian is quadratic in bosonic or fermionic creation and annihilation operators, with no further non-linear interactions present. For these 'non-interacting' models, the ETH approach is known to fail [50,52]. Yet, in the OQS approach, the convergence to the MGS has been proven analytically precisely for this class of Hamiltonians [10–13]. This provides a clear example that the two ways of describing thermalization refer to different physics, although, to our knowledge, a fair comparison between them has never been attempted.

Summary of results. To carry out this case study, we consider the physical model of a double quantum dot (DQD) coupled to a fermionic lead. The model is graphically illustrated in Figure 1. We present here an outline of our results, also summarised in Table 1, and refer to a more detailed discussion in the coming sections.

For the DQD+lead model, we construct typical initial states $|\psi(0)\rangle$, see details in Section 3.1. These allow us to explore both, the open quantum system (OQS) and the isolated quantum system (IQS) notions for thermalization in the same dynamics.

(1) We numerically evidence a crossover between OQS and IQS behaviors and identify a time scale t_{oqs}, proportional to the size of the bath $L_B \gg 1$, beyond which this crossover happens; see Section 3.3.1.

(2) We numerically confirm OQS thermalization on the time scale t_{oqs}, for both the free fermionic case ($V = 0$) and the interacting case ($V \neq 0$); see Section 3.3.2. Note that there is no mathematical proof for such thermalization when $V \neq 0$.

(3) We confirm that integrability of the DQD+lead system is broken for $V \neq 0$ by evidencing level repulsion, a crucial feature of non-integrability. However, looking at the full level-spacing distribution for the largest numerically accessible system size for exact diagonalization, we find that it shows significant differences to the Wigner-Dyson distribution

DQD+lead Hamiltonian	$\hat{H}(L_B) = \boxed{g\,(\hat{c}_1^\dagger \hat{c}_2 + \hat{c}_2^\dagger \hat{c}_1) + V\,\hat{n}_1\hat{n}_2}$ $+$ $\boxed{\gamma\,(\hat{c}_2^\dagger \hat{b}_1 + \hat{b}_1^\dagger \hat{c}_2)}$ $+$ $\boxed{g_B \sum_{\ell=1}^{L_B-1} (\hat{b}_\ell^\dagger \hat{b}_{\ell+1} + \hat{b}_{\ell+1}^\dagger \hat{b}_\ell)}$		
	$\hat{H}_S$ [DQD w. interaction V] $\quad\hat{H}_{SB}$ [DQD-lead coupling] $\quad\hat{H}_B(L_B)$ [fermionic lead (bath)]		
DQD+lead initial state	$\vert\psi(0)\rangle = \dfrac{e^{-\beta \hat{H}^{\mathrm{ini}}(L_B)/2}}{\sqrt{Z^{\mathrm{ini}}(L_B)}} \sum_{n=1}^{D} (a_n + i b_n)\vert\chi_n\rangle$	with initial decoupled Hamiltonian $\hat{H}^{\mathrm{ini}}(L_B) = \hat{H}_S^{\mathrm{ini}} + \hat{H}_B(L_B)$ and random Gaussian distributed weights a_n, b_n for basis states $\vert\chi_n\rangle$	
different regimes ①	**OQS regime**	**IQS regime**	
	$t \leq t_{\mathrm{oqs}}$ $\quad$ with $\quad t_{\mathrm{oqs}} = \dfrac{L_B - L_0}{g_B}$	$t \gg t_{\mathrm{oqs}}$	
thermalization statement	$\lim\limits_{L_B\to\infty} \hat{\rho}_S(t_{\mathrm{oqs}}; L_B) = \hat{\rho}_{\mathrm{MGS}}$ for reduced system state $\hat{\rho}_S$	$\overline{\langle\hat{A}\rangle} = A(E) + \mathcal{O}(L_B^{-1})$ $\overline{\delta\langle\hat{A}\rangle^2} \leq C\,e^{-\alpha L_B}$	for time-averaged expectation value and variance of local observables $\hat{A}$
$V = 0$ (free fermions)	thermalization statement **satisfied** ②	integrable ③	thermalization statement **not** satisfied ④
$V > 0$ (interacting case)	thermalization statement **satisfied**	**non-integrable***	thermalization statement **satisfied**

Table 1: Summary of model and four results, see main text for details.

expected for non-integrable systems; see Appendix A. To highlight this difference from full non-integrable behavior, we refer to this model as non-integrable*.

(4) Finally, we obtain numerical results for the dynamics at times $t \gg t_{\mathrm{oqs}}$, showing that thermalization in the IQS sense is indeed obeyed for the interacting case ($V \neq 0$); see Section 3.4.2. As expected, no such IQS thermalization occurs in the free fermionic case $V = 0$, contrasting with the OQS thermalization found at earlier times.

These results demonstrate that both the OQS and IQS thermalization statements can be assessed for the DQD coupled to the fermionic lead, putting the emphasis on the crucial role of the time-scale separation and the order of limits. For times $t \leq t_{\mathrm{oqs}} \propto L_B$ the DQD follows the thermalization process described by the OQS approach. For much longer times $t \gg t_{\mathrm{oqs}}$ thermalization happens as characterized by the IQS statements, provided the system is not integrable.

2 Setting and OQS vs. IQS approaches to thermalization

In this section, we introduce the specific physical model considered here as an illustrative example, as well as the general open quantum system (OQS) and isolated quantum systems (IQS) approaches to describe the dynamics of a quantum system.

2.1 Double quantum dot (DQD) coupled to fermionic lead

We consider the dynamics of a DQD coupled to a fermionic chain of length L_B, see Fig. 1. The global Hamiltonian is

$$\hat{H}(L_B) = \hat{H}_S + \hat{H}_{SB} + \hat{H}_B(L_B), \tag{1}$$

where

$$\hat{H}_S = g\,(\hat{c}_1^\dagger \hat{c}_2 + \hat{c}_2^\dagger \hat{c}_1) + V\,\hat{n}_1 \hat{n}_2, \tag{2}$$

$$\hat{H}_{SB} = \gamma\,(\hat{c}_2^\dagger \hat{b}_1 + \hat{b}_1^\dagger \hat{c}_2), \tag{3}$$

$$\hat{H}_B(L_B) = g_B \sum_{\ell=1}^{L_B-1} (\hat{b}_\ell^\dagger \hat{b}_{\ell+1} + \hat{b}_{\ell+1}^\dagger \hat{b}_\ell). \tag{4}$$

The operator $\hat{H}_S$ describes the Hamiltonian of the bare DQD, the 'system', which consists of two fermionic sites representing two quantum dots. Here $\hat{c}_p$ for $p = 1, 2$ is the fermionic annihilation operator of the p-th site, and $\hat{n}_p = \hat{c}_p^\dagger \hat{c}_p$ are the fermionic occupation number operators. The hopping amplitude between the two quantum dots is given by g, while $V > 0$ gives the repulsive many-body interaction between the two dots.

The second site of the DQD is coupled to a 'bath': a chain of nearest neighbour tight-binding fermions with L_B sites. The bath Hamiltonian is $\hat{H}_B(L_B)$, with intra-bath hopping constant g_B. Here $\hat{b}_\ell$ denotes the fermionic annihilation operator of the ℓ-th site of the bath. The coupling between the system and the bath is given by the interaction operator $\hat{H}_{SB}$, which is just a hopping term between the second site of the system and the first site of the bath, with hopping strength γ.

Apart from the V-repulsion term in the DQD, all other terms in $\hat{H}(L_B)$ are quadratic in fermion creation and annihilation operators. Therefore, $V = 0$ corresponds to free fermions. However, when $V \neq 0$, then a fourth order many-body interaction term is present in the Hamiltonian, and we will refer to this case as the *interacting DQD*. In the following, we discuss the notion of thermalization in both open quantum system (OQS) and isolated quantum system (IQS) approaches, highlighting their differences, and pointing out how our setting can correspond to both.

2.2   OQS thermalization

This section provides general background on the OQS approach applicable for any system-bath Hamiltonian [23–26]. Consider an initial system-bath state of product form $\hat{\rho}_S(0) \frac{e^{-\beta \hat{H}_B}}{Z_B}$, in which the system is in any state $\hat{\rho}_S(0)$, and the bath is in a thermal equilibrium state with respect to the bath's bare Hamiltonian $\hat{H}_B(L_B)$ at inverse temperature β, with bath partition function $Z_B = \mathrm{Tr}_B\left(e^{-\beta \hat{H}_B}\right)$. Since our setting has conservation of number of particles, a more general initial state would consider a chemical potential for the bath. In this paper, for simplicity, we set the chemical potential to zero. The dynamics of the DQD is obtained by tracing out the bath degrees of freedom of the full density matrix at time t,

$$\hat{\rho}_S(t; L_B) = \mathrm{Tr}_B\left[e^{-it\hat{H}(L_B)}\,\hat{\rho}_S(0)\frac{e^{-\beta \hat{H}_B(L_B)}}{Z_B}\,e^{it\hat{H}(L_B)}\right], \tag{5}$$

where we set $\hbar = 1$. The DQD state in the thermodynamic limit, $L_B \to \infty$, is denoted by

$$\hat{\rho}_S(t) = \hat{\Lambda}(t)\left[\hat{\rho}_S(0)\right] = \lim_{L_B \to \infty} \hat{\rho}_S(t; L_B), \tag{6}$$

which defines $\hat{\Lambda}(t)$, a completely positive trace preserving map on system density matrices. All standard techniques in OQS theory, like quantum master equations, non-equilibrium Green's functions, the Feynman Vernon influence functional, Keldysh-Schwinger path integrals, quantum Langevin equations etc. [23, 25, 26, 28], are formalisms to describe the dynamics of $\hat{\rho}_S(t)$ under this completely positive trace preserving map. For all these OQS techniques, taking the limit

$L_B \to \infty$ is crucial, because it is in this limit that the bath becomes a continuum of fermionic modes and the dynamics becomes dissipative (irreversible).

We now discuss the thermodynamic limit $L_B \to \infty$ for the bath Hamiltonian $\hat{H}_B(L_B)$, (4). It is useful to go to the single particle eigenbasis of the bath by diagonalizing the tight-binding chain. The bath Hamiltonian and the system-bath coupling Hamiltonian then become

$$\hat{H}_B = \sum_{r=1}^{L_B} \Omega_r \hat{B}_r^\dagger \hat{B}_r \text{ with } \Omega_r = 2g_B \cos\left(\frac{\pi r}{L_B + 1}\right) \text{ and } \hat{H}_{SB} = \sum_{r=1}^{L_B} \kappa_r \left(\hat{c}_2^\dagger \hat{B}_r + \hat{B}_r^\dagger \hat{c}_2\right), \quad (7)$$

$$\text{where } \hat{B}_r = \sum_{\ell=1}^{L_B} \Phi_{\ell r} \, \hat{b}_\ell \quad \text{with} \quad \Phi_{\ell r} = \sqrt{\frac{2}{L_B + 1}} \sin\left(\frac{\pi \ell r}{L_B + 1}\right) \quad \text{and} \quad \kappa_r = \gamma \Phi_{1r}. \quad (8)$$

In the above, $\hat{B}_r$ is the annihilation operator for the r-th mode of the bath. It is a standard fact from OQS theory [23,25,26,28] that for such a linearly coupled system and in the $L_B \to \infty$ limit, the influence of the bath on the system dynamics (DQD) is entirely governed by the bath spectral function, also called the hybridization function, defined as

$$\mathfrak{J}(\omega) = 2\pi \lim_{L_B \to \infty} \sum_{r=1}^{L_B} |\kappa_r|^2 \delta(\omega - \Omega_r). \quad (9)$$

In other words, $\hat{\Lambda}(t)$ depends on the bath Hamiltonian parameters only through the quantity $\mathfrak{J}(\omega)$. Using Eq. (7) and (8) in Eq. (9), and converting the summation to an integral taking $q = (\pi r)/(L_B + 1)$ and $dq = \pi/(L_B + 1)$, the bath spectral function for (7) is found to be

$$\mathfrak{J}(\omega) = 4\gamma^2 \int_0^\pi dq \, \sin^2(q) \, \delta(\omega - 2g_B \cos q) = \frac{2\gamma^2}{g_B} \sqrt{1 - \left(\frac{\omega}{2g_B}\right)^2} \quad \text{for } |\omega| \leq 2g_B, \quad (10)$$

and $\mathfrak{J}(\omega) = 0$ for $|\omega| > 2g_B$.

Typically, due to the contact with the bath, the evolution of the system is driven to a stationary state, or steady state, in the long time limit, provided that the system-bath interaction is 'effective', allowing for energy exchange processes between the two components, and the bath is in the thermodynamic limit. This is usually guaranteed to happen if the bath spectral function does not vanish at the Bohr (transition) frequencies of the system, ensuring that bath quanta can induce transitions in the system by absorption and emission processes. This is a general feature of open systems, discussed for example in [12, 16, 17, 20–24]. In such situations, the long-time steady state is very often unique, i.e, independent of the initial state of the system. We will only consider parameter regimes where there is a unique steady state.

Given this setting, the statement of thermalization in the OQS approach is:

$$\lim_{t \to \infty} \left(\lim_{L_B \to \infty} \hat{\rho}_S(t; L_B)\right) = \hat{\rho}_{\text{MGS}}, \quad (11)$$

where we recall the definition of the reduced density matrix $\hat{\rho}_S(t; L_B)$ in (5), and where the *mean force Gibbs state* is defined by

$$\hat{\rho}_{\text{MGS}} = \lim_{L_B \to \infty} \text{Tr}_B\left[\frac{e^{-\beta \hat{H}(L_B)}}{Z(L_B)}\right], \quad (12)$$

with total partition function $Z(L_B) = \text{Tr}\left[e^{-\beta \hat{H}(L_B)}\right]$. In other words, the state of the system should converge to the mean force Gibbs state in the long time and thermodynamic limits of the

set-up, irrespective of the initial state of the system. However, it is important to note the order of limits. In the OQS approach, the system is expected to converge to its asymptotic, mean force Gibbs state if *first* one takes the large bath limit, $L_B \to \infty$, and *afterwards* one takes the long time limit, $t \to \infty$.

We note that although the above statement of OQS thermalization is expected to hold generally, so far it has only been proven for special cases. These include free fermionic and free bosonic models [7–13] and a range of results in the regime of ultraweak and weak coupling between system and bath [7, 9, 18–23, 36, 38, 62–67]. Hence it becomes important to numerically check the notion of thermalization of OQS beyond weak system-bath coupling and with non-linear interactions present, where analytical proofs that OQS thermalization occurs are lacking. The task will thus be to check for the validity of Eq. (11) for the DQD in the presence of the non-linear V interaction, see Fig. 1.

2.3 IQS thermalization

Now turning to the isolated quantum system (IQS) approach, here one does not make a distinction between the DQD and the fermionic lead. Rather, one considers the two together as an isolated system. Now, an observable $\hat{A}$, that is, in our case, an operator acting on the whole DQD plus fermionic lead, is called *local* if it acts non-trivially on a fixed set of sites, independently of how large we take L_B, or is a sum of such observables. For example, observables acting on the first two sites (on the DQD, see. Fig. 1) are local.

To state the thermalization in the IQS approach, we look at the expectation value of the local operator $\hat{A}$ as a function of time

$$\langle \hat{A}(t) \rangle = \langle \psi | e^{i\hat{H}t} \hat{A} e^{-i\hat{H}t} | \psi \rangle. \tag{13}$$

The initial state $|\psi\rangle$ is supposed to have a small energy spread around the given value $E = \langle \psi | \hat{H} | \psi \rangle$. This is usually quantified as [50]

$$\frac{\langle \psi | \hat{H}^2 | \psi \rangle - \langle \psi | \hat{H} | \psi \rangle^2}{\langle \psi | \hat{H} | \psi \rangle^2} \sim O(L_B^{-1}). \tag{14}$$

We denote by $A(E)$ the expectation value of $\hat{A}$ in the microcanonical ensemble at energy E [68]. From the equivalence of ensembles in standard statistical physics, one has

$$A(E) = \lim_{L_B \to \infty} \text{Tr} \left[\hat{A} \frac{e^{-\beta_E \hat{H}}}{Z} \right], \tag{15}$$

where the microcanonical entropy S at energy E is used to define the microcanonical inverse temperature,

$$\beta_E = \frac{\partial S(E)}{\partial E}. \tag{16}$$

In this setting, the statement of thermalization in the IQS approach now is [4, 39–46, 49–56]

$$\overline{\langle \hat{A} \rangle} := \lim_{t \to \infty} \frac{1}{t} \int_0^t dt' \langle \hat{A}(t') \rangle = A(E) + \mathcal{O}(L_B^{-1}), \tag{17}$$

$$\overline{\delta \langle \hat{A} \rangle^2} := \lim_{t \to \infty} \frac{1}{t} \int_0^t dt' \left| \langle \hat{A}(t') \rangle - \overline{\langle \hat{A} \rangle} \right|^2 \leq C e^{-\alpha L_B}. \tag{18}$$

The first equalities in (17) and (18) are definitions. The second equality in (17) and the inequality in (18) defines the meaning of thermalization in IQS. In Eq. (18), the constants C and α are non-universal positive constants which are independent of L_B.

Equation (17) says that the infinite time average of the expectation value deviates from its value obtained from the microcanonical ensemble by a small term, having size at most of the order of L_B^{-1}. The second IQS thermalization statement (18) says that time-averaged fluctuations about the infinite time average are exponentially small in L_B, in the long time limit. These two statements combined say that for large times, the time-averaged expectation value of the local observable approaches its (infinite time) mean value modulo exponentially small fluctuations in L_B.

For large enough values of L_B, and since, in our example, the DQD consists of only the first two sites of chain (see. Fig. 1), the inverse temperature β_E in Eq. (16) depends minimally on the initial state of the DQD, and equals to a very good approximation the fermionic lead's inverse temperature β, governed by the lead's initial state. Then, for local operators $\hat{A}_S$ that only act on the DQD Hilbert space, the IQS statement of thermalization given in Eq.(17) becomes

$$\overline{\langle \hat{A}_S \rangle} = A_{\mathrm{MGS}} + \mathcal{O}(L_B^{-1}), \tag{19}$$

where A_{MGS}, defined as

$$A_{\mathrm{MGS}} = \mathrm{Tr}\left[\hat{A}_S \, \hat{\rho}_{\mathrm{MGS}}\right], \tag{20}$$

is the expectation value of $\hat{A}_S$ in the mean force Gibbs state (12). The inverse temperature β appearing in the state ρ_{MGS} is the inverse temperature obtained from initial state of the fermionic lead. Due to the small contribution to the total energy stemming from the interaction between the DQD and the fermionic lead, beyond a minimal lead size L_B, the value of A_{MGS} will remain approximately constant under further increase of L_B.

Considering local observables on the DQD, and combining Eq. (19) with Eqs. (17) and (18), we see that thermalization in the IQS approach also means convergence of the state of the DQD to $\hat{\rho}_{\mathrm{MGS}}$, in the long time and thermodynamic limit. At first sight this appears similar to thermalization in the OQS approach. However, there are crucial differences, which we describe below.

2.4 Distinguishing OQS and IQS thermalization

The main difference between the OQS and IQS notions of thermalization is the order in which the long time and the thermodynamic limits are taken. The OQS thermalization refers to convergence to $\hat{\rho}_{\mathrm{MGS}}$ when the thermodynamic limit ($L_B \to \infty$) is taken first, and then the long-time limit ($t \to \infty$) is taken (see Eq. (11)). In the IQS approach, first an infinite time average of any observable is taken for a fixed finite L_B. The statements of the IQS thermalization tell us how this value approaches the corresponding value obtained from $\hat{\rho}_{\mathrm{MGS}}$, and how the fluctuations about the latter decay, with increasing L_B (see Eqs.(17),(18)).

This difference has important consequences. In most of the literature, thermalization in the IQS approach is discussed for quantum many-body systems, i.e, in the presence of many-body interactions [4,39–61]. In particular, the most well-accepted mechanism for IQS thermalization is the so-called eigenstate thermalization hypothesis (ETH) [1–3, 5, 44, 50], which is expected to apply to non-integrable quantum systems. Thermalization in the IQS has been numerically established in a range of quantum non-integrable many-body systems [4, 44, 47, 48, 50, 52, 53, 55, 56, 58, 60]. The requirement of non-integrability excludes cases such as free fermions and free bosons, where many-body interaction terms are absent in the Hamiltonian. ETH does not apply and IQS thermalization is not expected to occur in such systems. This is in stark contrast with the fact that proofs for the OQS thermalization are known only for free fermionic and free bosonic systems [7–13, 16–22]. Thus it may appear that the two notions of thermalization are at odds with each other, predicting that the same system does or does not thermalize. In the current work, we resolve this seeming inconsistency.

Recalling the concepts of OQS and IQS thermalizations discussed in Secs. 2.2 and 2.3 above, there seems to be a second key difference: while OQS thermalization is discussed for initial states of the whole set-up that are mixed, IQS thermalization is usually discussed for initial pure states. As we will discuss in Sec. 3.1 below, this difference can be completely bridged. Before we get to that, we next outline how to obtain the state of the DQD as a function of time.

2.5 Obtaining the density matrix of the DQD

To present the equilibration results for the OQS and the IQS approach in section 3, we use four local DQD operators which fully describe the DQD state, as we explain now.

For any initial state $\hat{\rho}(0)$ of the DQD plus the fermionic leads, see Eq. (5), the reduced DQD density matrix at time t is given by

$$\hat{\rho}_S(t; L_B) = \text{Tr}_B \left[e^{-it\hat{H}(L_B)} \hat{\rho}(0) e^{it\hat{H}(L_B)} \right]. \tag{21}$$

The global Hamiltonian $\hat{H}(L_B)$ is number conserving, i.e., it commutes with the total number operator $\hat{N}_{\text{tot}} = c_1^\dagger c_1 + c_2^\dagger c_2 + \sum_{\ell=1}^{L_B} b_\ell^\dagger b_\ell$. We will denote the total number of excitations as N. When the initial state $\hat{\rho}(0)$ also commutes with the total number operator

$$[\hat{\rho}(0), \hat{N}_{\text{tot}}] = 0, \tag{22}$$

then the reduced density matrix $\hat{\rho}_S(t; L_B)$ leaves the sectors of a fixed number (0 or 1 or 2) of excitations of the DQD invariant. In this case the time-evolved DQD density matrix is of the form

$$\hat{\rho}_S(t; L_B) = \begin{bmatrix} \rho_{00,00}(t) & 0 & 0 & 0 \\ 0 & \rho_{01,01}(t) & \rho_{01,10}(t) & 0 \\ 0 & \rho_{10,01}(t) & \rho_{10,10}(t) & 0 \\ 0 & 0 & 0 & \rho_{11,11}(t) \end{bmatrix}, \tag{23}$$

written in the ordered orthonormal basis $\{|00\rangle, |01\rangle, |01\rangle, |11\rangle\}$ of the DQD Hilbert space, labeling the excitations of the two DQD sites. Using the notation

$$\langle \hat{A}(t) \rangle := \text{Tr} \left[\hat{A} \, e^{-it\hat{H}(L_B)} \, \hat{\rho}(0) \, e^{it\hat{H}(L_B)} \right], \tag{24}$$

the matrix elements of (23) are expressed entirely in terms of the expectations of the four DQD operators

$$\langle \hat{n}_1(t) \rangle, \ \langle \hat{n}_2(t) \rangle, \ \langle \hat{c}_1^\dagger(t) \hat{c}_2(t) \rangle, \ \langle \hat{n}_1(t) \hat{n}_2(t) \rangle, \tag{25}$$

which of course depend on the bath size L_B. Explicity, we have

$$\begin{aligned} \rho_{01,10}(t) &= \rho_{10,01}^*(t) = \langle \hat{c}_1^\dagger(t) \hat{c}_2(t) \rangle \\ \rho_{11,11}(t) &= \langle \hat{n}_1(t) \hat{n}_2(t) \rangle \\ \rho_{01,01}(t) &= \langle \hat{n}_1(t) \rangle - \langle \hat{n}_1(t) \hat{n}_2(t) \rangle \\ \rho_{10,10}(t) &= \langle \hat{n}_2(t) \rangle - \langle \hat{n}_1(t) \hat{n}_2(t) \rangle \\ \rho_{00,00}(t) &= 1 - \rho_{10,10}(t) - \rho_{01,01}(t) - \rho_{11,11}(t). \end{aligned} \tag{26}$$

In this paper, we will consider states satisfying Eq. (22) for all our analysis, without further mention.

3 Results

In this Section we present our main results, which were summarised in Table 1 above.

3.1 Treating OQS and IQS on same footing via dynamical typicality

We first explain the concept of dynamical typicality and then we show how we can use that to treat both the OQS and the IQS formalisms on the same footing.

Let $\{|\chi_n\rangle\}_{n=1}^{D_{\text{tot}}}$ be an arbitrary orthonormal basis of the entire system plus bath Hilbert space of dimension $D_{\text{tot}} = 2^{L_B+2}$. Let also a_n and b_n be independent, identically distributed random numbers with Gaussian distribution of mean 0 and variance $1/2$. A state of the form

$$|\psi\rangle = \hat{R} \sum_{n=1}^{D_{\text{tot}}} (a_n + ib_n)|\chi_n\rangle, \tag{27}$$

where $\hat{R}$ is an arbitrary linear operator in the Hilbert space, is called a *typical state* [69, 70]. Denote by $\mathbb{E}$ the average (expectation) with respect to the Gaussian distribution of the a_n, b_n. It can be verified that for any observable $\hat{A}$ we have $\mathbb{E}[\langle\psi|\hat{A}|\psi\rangle] = \text{Tr}[\hat{R}\hat{R}^\dagger\hat{A}]$ [69,70]. If $\hat{R}$ is chosen such that $\hat{R}\hat{R}^\dagger$ is a density matrix, then the last equality means that the expectation value of operator $\hat{A}$ averaged over the ensemble of pure states $|\psi\rangle$ is the same as taking the quantum-mechanical average of $\hat{A}$ in the state $\hat{\rho} = \hat{R}\hat{R}^\dagger$. Moreover, if $\text{Tr}[\hat{\rho}^2] \ll 1$, i.e, if the density matrix $\hat{\rho}$ is sufficiently mixed, then the sample to sample fluctuations coming from the Gaussian distribution of the a_n, b_n, decay as $\sim D_{\text{tot}}^{-1}$ [69, 70]. Since, in the current model, $D_{\text{tot}} = 2^{L_B+2}$, those fluctuations are exponentially suppressed with increase in the lattice size L_B. Therefore, for large L_B, operator expectation values obtained from a *single realization* of the typical state $|\psi\rangle$ closely approximate those obtained from the ensemble averaged state $\hat{\rho} = \hat{R}\hat{R}^\dagger$,

$$\langle\psi|\hat{A}|\psi\rangle \sim \text{Tr}[\hat{\rho}\hat{A}]. \tag{28}$$

Here the $\sim$ sign means that a single realization gives an operator expectation value very close to that obtained for the Gaussian averaged state. This is the statement of *dynamical typicality* [69, 70].

Our main idea here is to use dynamical typicality to pass between pure initial states used in the formulation of the IQS approach (Section 2.3) and mixed (equilibrium) initial states used in the OQS approach (Section 2.2). We will therefore use, for both the OQS and IQS approaches, initial states of the form

$$|\psi(0)\rangle = \frac{e^{-\beta\hat{H}^{\text{ini}}(L_B)/2}}{\sqrt{Z^{\text{ini}}(L_B)}} \sum_{n=1}^{D_{\text{tot}}} (a_n + ib_n)|\chi_n\rangle, \tag{29}$$

where $Z^{\text{ini}}(L_B)$ is a normalization constant. The operator in front of the sum in (29) is the square root of the thermal density matrix associated with the uncoupled system-bath Hamiltonian

$$\hat{H}^{\text{ini}}(L_B) = \hat{H}_S^{\text{ini}} + \hat{H}_B(L_B), \tag{30}$$

where the fermionic lead Hamiltonian $\hat{H}_B(L_B)$ is given in (4). Furthermore, $\hat{H}_S^{\text{ini}}$ is a new initial-state system-Hamiltonian, defined by

$$\hat{H}_S^{\text{ini}} = \varepsilon_1^{\text{ini}} \hat{n}_1 + \varepsilon_2^{\text{ini}} \hat{n}_2 + g^{\text{ini}} \left(e^{i\phi^{\text{ini}}} \hat{c}_1^\dagger \hat{c}_2 + e^{-i\phi^{\text{ini}}} \hat{c}_2^\dagger \hat{c}_1 \right) + V^{\text{ini}} \hat{n}_1 \hat{n}_2, \tag{31}$$

where the parameters $\varepsilon_{1,2}^{\text{ini}}$, g^{ini}, ϕ^{ini} and V^{ini} are arbitrary real numbers.

According to (28), applied to the observable $\hat{A}(t) = e^{it\hat{H}(L_B)}\hat{A}e^{-it\hat{H}(L_B)}$, the dynamics of expectation values starting in the pure initial state in Eq. (29) (for any randomly chosen values of a_n, b_n and L_B large) is indistinguishable from the dynamics starting in the total mixed state

$$\hat{\rho}(0) = \frac{e^{-\beta\hat{H}^{\text{ini}}(L_B)}}{Z^{\text{ini}}(L_B)} = \hat{\rho}_S(0)\frac{e^{-\beta\hat{H}_B(L_B)}}{Z_B(L_B)} \tag{32}$$

where $Z^{\text{ini}}(L_B) = Z_S^{\text{ini}}Z_B(L_B)$ and the initial system state is expressed as $\hat{\rho}_S(0) = \frac{e^{-\beta\hat{H}_S^{\text{ini}}}}{Z_S^{\text{ini}}}$. The initial state $\hat{\rho}(0)$ is thus a product of the DQD and the fermionic lead, where the lead always starts in a thermal state at inverse temperature β. Varying over the parameters in $\hat{H}_S^{\text{ini}}$ allows us to describe *arbitrary* initial states of the DQD, which furthermore commute with the number of particles in the DQD. Note that $\hat{\rho}(0)$ commutes with the operator of total number of excitations, $\hat{N}_{\text{tot}}$ (see also(22)). We consider $\hat{\rho}(0)$ as a grandcanonical density matrix with $\mu = 0$, rather than a canonical density matrix $\hat{\rho}_N(0)$ in a fixed number sector of excitations N, i.e.

$$\hat{\rho}(0) = \sum_{N=0}^{L_B+2}\frac{e^{\beta\mu N}\hat{\rho}_N(0)}{\sum_{k=0}^{L_B+2}e^{\beta\mu k}} \quad \text{which for } \mu = 0 \text{ becomes}: \hat{\rho}(0) = \frac{1}{L_B+3}\sum_{N=0}^{L_B+2}\hat{\rho}_N(0). \tag{33}$$

This means that for simulations starting from the typical state (29) we average over all number sectors. This contrasts with many studies on ETH where only the half-filled sector (i.e. $N = \frac{L_B}{2}+1$) is considered. This is important for the fair comparison because standard OQS thermalization considers grandcanonical density matrices.

Finally we note that $\hat{\rho}(0)$ in Eq.(32) is a thermal state of a short range Hamiltonian, which differs from $\hat{H}(L_B)$ only in the first two sites. By virtue of equivalence of ensembles of statistical physics, this guarantees that $\hat{\rho}(0)$ has a small spread in energy. The analog of Eq. (14) is then satisfied for the expectation values for the mixed state $\hat{\rho}(0)$ obtained from the Hamiltonian $\hat{H}^{\text{ini}}(L_B)$. The same will hold when calculating the expectation values with respect to $\hat{H}(L_B)$ instead. Since this is the same as obtaining the expectation values from $|\psi(0)\rangle$ in Eq. (29), our choice of initial state satisfies Eq. (14). We have also confirmed this numerically.

Thus, for exploring both OQS and IQS thermalization, we need to evolve the state $|\psi(0)\rangle$ in Eq. (29) to a long time using the full Hamiltonian of DQD and the fermionic lead, for finite but large enough L_B. We need to obtain the four DQD expectation values given in Eq. (25) as a function of time. Obtaining such data for various values of L_B allows us to check both OQS thermalization [Eq. (11)] and IQS thermalization [Eqs. (17), (18), (19)]. We require neither separate models nor separate initial states to consider thermalization in OQS and IQS approaches. Rather, as we establish later, we only need to consider separate time regimes of the same data obtained from the same model starting with the same initial state. This allows a fair comparison of the two approaches to thermalization and highlights the difference between the two.

Numerical technique. Before we present our numerical results, we here briefly comment on how the numerics were carried out. As mentioned in Sections 2.2 and 2.3, for both the OQS and IQS approaches, one must consider large bath sizes L_B and simulate the dynamics up to long enough times. For $V \neq 0$, free-fermion techniques do not apply and numerical implementations are hard because the Hilbert space dimension D scales exponentially with L_B. Nevertheless, the global Hamiltonian Eq. (1) describes a nearest neighbour tight-binding chain of spinless fermions, with nearest neighbour many-body interaction only between the first two sites. Written in the Fock state basis, the Hamiltonian is block diagonal because number of particles is conserved. Additionally, it is a sparse matrix. Within our computational resources, exact diagonalization is possible up to $L_B = 18$ (total chain length is 20 sites). However, this size is not large enough to
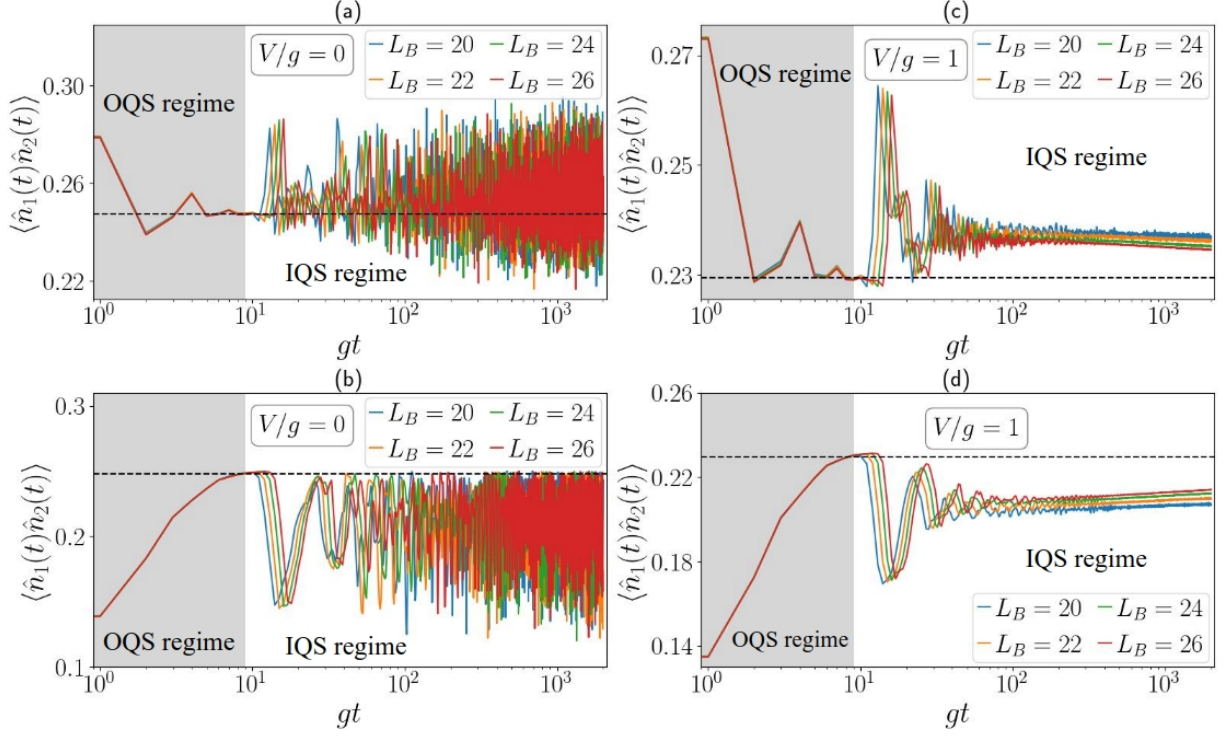
Figure 2:   *Crossover between OQS and IQS regimes:* Shown is the dynamics of a representative DQD observable, $\langle \hat{n}_1(t)\hat{n}_2(t)\rangle$, for different bath sizes L_B, starting from an initial state of the form in Eq. (29), with two different sets of randomly chosen parameters in $\hat{H}_S^{\text{ini}}$, see Eq. (31), corresponding to two randomly chosen initial reduced states for the DQD. The left panels, (a) and (b), show the dynamics for the free model ($V = 0$) for the two different initial condition of the DQD. Panels (c) and (d) show the dynamics for the interacting model ($V = g$), for the same two initial condition of the DQD as above. The horizontal dashed lines show the expectation values of the mean force Gibbs state $\hat{\rho}_{\text{MGS}}$ corresponding to the cases $V = 0$ and $V = g$, respectively. The x-axis is shown on log-scale to capture features over a wide time regime. The shaded region corresponds to the time up to which plots for various L_B overlap, which is the OQS regime. In the remaining time regime, which we denote the IQS regime, the DQD feels the finiteness of L_B. The data in the OQS regime shows strong evidence of OQS thermalization for both $V = 0$ and $V = g$. The data in the IQS regime shows strong evidence of IQS thermalization for $V = g$, as we discuss in the following sections in the main text. Other parameters: $g_B = 2g$, $\gamma = g$, $\beta g = 0.1$.

clearly demonstrate all of the effects we wish to explore. We thus use the Chebyshev polynomial method [71–74], in which the dynamics can be simulated without diagonalizing the Hamiltonian, but rather repeatedly using sparse matrix vector multiplications. The initial state in Eq. (29) can also be prepared similarly, using imaginary time evolution. With this method, we can reach up to $L_B = 26$ within our computational resources (total chain length is 28 sites, size of the largest block of Hamiltonian in Fock space is $40,116,600$). More importantly, it allows the simulation up to extremely long times (up to $\sim 2000gt$). The chain sizes and times treatable with this method are large enough to clearly explore both OQS and IQS regimes, as we see next.

3.2　Numerical results: OQS to IQS crossover in the same dynamics

We now show numerical results obtained via the procedure detailed in the previous subsection. To simulate the dynamics starting from an arbitrary, but fixed, initial state of the DQD we choose a set of random parameters in $\hat{H}_S^{\text{ini}}$. In Fig. 2 we show plots of the dynamics of a representative observable of the DQD for various values of L_B, starting from two different initial conditions, and for the cases $V = 0$ and $V = g$. In all four cases, we see that the value of L_B hardly affects the dynamics up to some time. Thus, within this time, the DQD does not feel the finiteness of L_B. The dynamics in this regime therefore corresponds to the $L_B \to \infty$ case, and hence to the OQS case. The expectation values in this regime show clear relaxation dynamics towards those obtained with $\hat{\rho}_{\text{MGS}}$, irrespective of the initial state. This is true for both $V = 0$ and $V = g$, as expected for OQS thermalization.

Beyond this regime, the finiteness of L_B is seen. We call this the IQS regime, because the usual assumption of a bath with infinite degrees of freedom does not hold here. In this regime, the nature of the dynamics differs greatly for $V = 0$ and $V = g$. For $V = g$ we see clear signatures of relaxation, while for $V = 0$, we do not see the same within the available values of L_B. As we show later, the data for $V = g$ in this regime show strong signature of IQS thermalization.

This clear crossover from OQS behavior to IQS behavior in the same dynamics at different time scales is our first and main result. In the following, we analyze the numerical results in the OQS and the IQS regimes in more detail.

3.3　Thermalization in the OQS regime

We now discuss the equilibration dynamics of the DQQ in contact with the fermionic lead, within the open quantum systems approach. To do this, we first discuss the relevant time-scale.

3.3.1　Relevant time-scale in the OQS approach

The fermionic lead plays the role of the bath for the DQD. This bath is a nearest neighbour tight-binding chain and only the first site of the bath is coupled to the DQD, see Fig. 1. At the initial time, the system-bath coupling is switched on. Due to the bath being a short-ranged lattice system, Lieb-Robinson bounds dictate that, at any finite time t, only a finite part of the bath is affected by this switching-on [75–77]. The 'disturbance' given by the switching-on of system-bath coupling spreads with the Fermi velocity, $v_F = 2g_B$ and reaches the site L_B in time $t_1 \simeq L_B/(2g_B)$. Then, it is reflected back. The DQD is influenced by the finite size of the bath when this reflected 'signal' reaches it. The reflected 'signal' again travels with Fermi velocity, so, the dynamics of the system is negligibly affected by the finiteness of the tight-binding chain representing the bath till $t \simeq 2t_1 \simeq L_B/g_B$. In practice, therefore, to exactly obtain the dynamics of the system in the presence of a macroscopic bath up to a time t, it suffices to consider a bath of size

$$L_B = g_B t + L_0, \tag{34}$$

where L_0 is a chosen fixed offset, independent of t and L_B. The fixed offset L_0 is chosen such that there is sufficiently small finite bath-size effect. We numerically find it sufficient to choose $L_0 = 8$. So, for our setting, the statement of thermalization in OQS approach,i.e, Eq. (11), can be recast as

$$\lim_{t\to\infty} \hat{\rho}_S(t; g_B t + L_0) = \lim_{L_B\to\infty} \hat{\rho}_S\left(\frac{L_B - L_0}{g_B}; L_B\right) = \hat{\rho}_{\text{MGS}}. \tag{35}$$

In particular, in the second equality above, the functional dependence of time on L_B ensures that the time is not long enough to resolve the discreteness of the bath energy levels, and the

DQD perceives the bath as a continuum. Combining all the discussion in this section and in Sec. 3.1, we see that, for our choice of initial state Eq.(29), for a given L_B and a chosen fixed L_0, the dynamics of the DQD up to time

$$t_{\text{oqs}} = \frac{L_B - L_0}{g_B} \tag{36}$$

corresponds to the OQS regime. In other words, for a finite bath of size L_B, the time t_{oqs} is the relevant timescale up to which the open system approach is suitable for describing equilibration.

Thermalization of the DQD in the OQS approach then corresponds to convergence of the state of the DQD to $\hat{\rho}_{\text{MGS}}$ within this regime, starting from a global initial pure state of the form given in Eq. (29). We re-iterate that, in this choice of initial state, the arbitrariness of the parameters in $\hat{H}_S^{\text{ini}}$ makes the initial state of the DQD arbitrary. The convergence should happen irrespective of the DQD initial state, i.e, irrespective of the choice of parameters in $\hat{H}_S^{\text{ini}}$. Such thermalization is expected to hold both for free fermion case ($V = 0$), and the interacting DQD case ($V \neq 0$). This is indeed the case, as we show numerically below.

3.3.2   Numerical evidence for thermalization in OQS regime

In Fig. 3, we analyze the numerical results for the same simulation as in Fig. 2, considering only early times, $t \leq t_{\text{oqs}}$. In particular, graphs (a) and (d) illustrate the correctness of Eq. (35), both for the free fermion case ($V = 0$, panels (a)–(c)) and the interacting case ($V \neq 0$, panels (d)–(f)).

Panels (a) and (d) of Fig. 3 show the dynamics of a representative observable $\langle \hat{n}_1(t)\hat{n}_2(t)\rangle$, see Eq. (25), in the regime $t \leq t_{\text{oqs}}$ with $t_{\text{oqs}}(L_B)$ given in (36), for various choices of L_B, and one choice of initial state $|\psi(0)\rangle$, see Eq. (29). One clearly sees that plots for smaller values of L_B overlap with those of larger values of L_B, demonstrating that there is no finite bath size effect in this regime. With increase in L_B, which leads to increase in t_{oqs}, the observable expectation value converges to that obtained from $\hat{\rho}_{\text{MGS}}$. Note, that $\hat{\rho}_{\text{MGS}}$ and hence the dashed lines depend on the value of V. In panels (b) and (e) of Fig. 3, we display the dynamics of $\langle \hat{n}_1(t)\hat{n}_2(t)\rangle$ in the regime $t \leq t_{\text{oqs}}$ for the two different randomly chosen initial states of the DQD (see Fig. 2), keeping $L_B = 26$. The plots clearly demonstrate that irrespective of its initial value, the average of the observable converges to its value in $\hat{\rho}_{\text{MGS}}$. This is the second result of the paper.

In panels (c) and (f) of Fig. 3, we further plot the trace distance T between $\hat{\rho}_S(t_{\text{oqs}}; L_B)$, i.e. the density matrix (21) of the DQD at time t_{oqs} specified in Eq. (36), and $\hat{\rho}_{\text{MGS}}$, i.e. the DQD's mean force Gibbs state (12), as a function of L_B for two different initial states of the DQD.[1] We find that the trace distance decays exponentially with L_B, directly evidencing the convergence of the state.

We would like to highlight that although convergence to $\hat{\rho}_{\text{MGS}}$ is expected in the OQS regime [7] for $V \neq 0$, no convergence proof exists. To our knowledge, such convergence has also not numerically been shown for any system with many-body interactions. Thus, the observation of dynamical convergence to $\hat{\rho}_{\text{MGS}}$ for the $V = g$ DQD is a new result, albeit perhaps not very surprising.

As we will see next, for a given L_B, the IQS regime is reached when the evolution is continued beyond time t_{oqs}, where only the interacting DQD case (and not the free fermion case) will show thermalization, in stark contrast with the OQS regime.

---

[1] The trace distance between any two density matrices $\hat{\rho}_1$ and $\hat{\rho}_2$ is defined as $T(\hat{\rho}_1, \hat{\rho}_2) = \frac{1}{2}\sum_{r=1}^{d} |\lambda_r|$, where λ_r, $r = 1, 2, 3, \ldots d$ are the eigenvalues of $\hat{\rho}_1 - \hat{\rho}_2$, and d is the Hilbert space dimension.
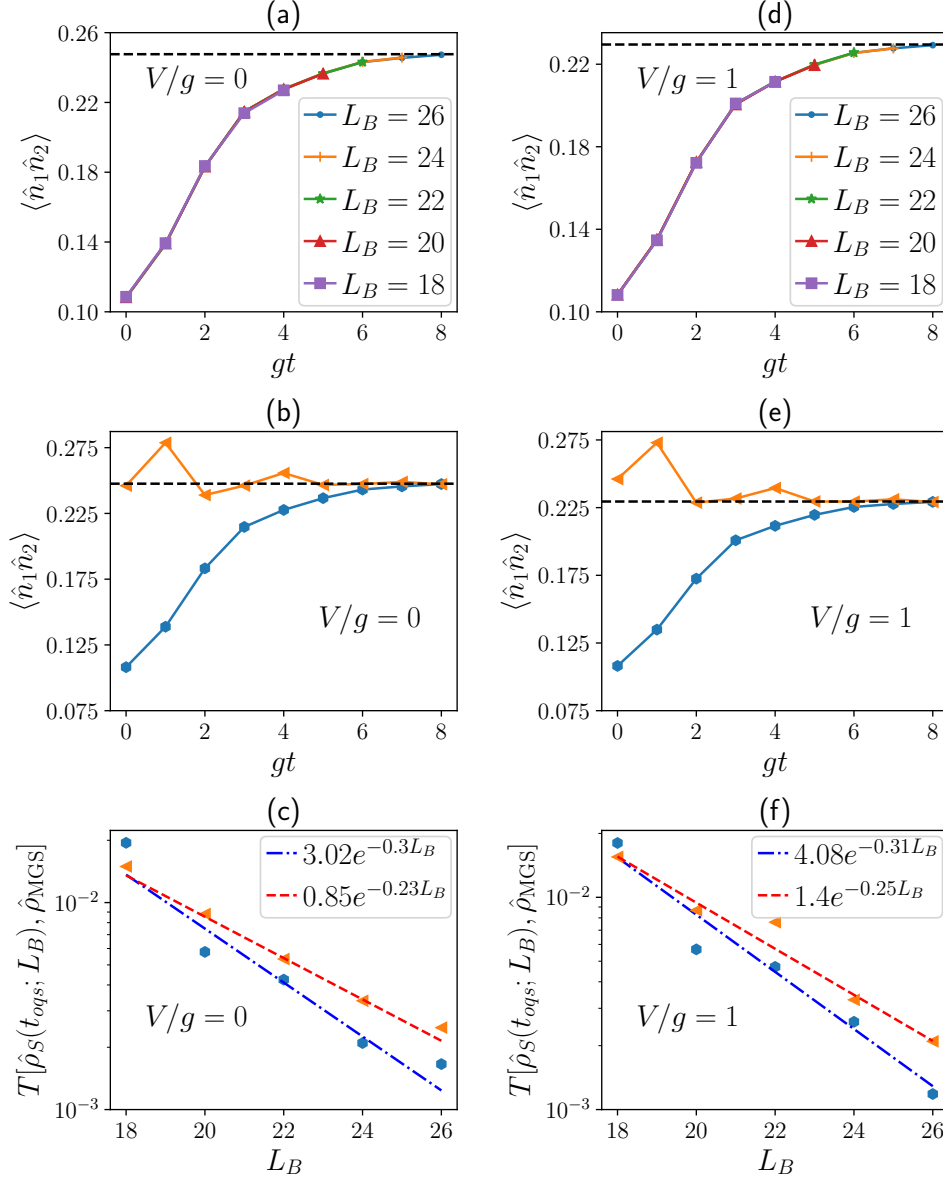
Figure 3: *Thermalization in the OQS regime:* Panels (a), (b), (c) are for the free fermion case, $V = 0$. Panels (d), (e), (f) are for the interacting DQD case with $V = g$. The results in (a), (d) corresponds to the same simulation as in Fig. 2(a) and (c), now plotted only for $t \leq t_{oqs}$, which corresponds to the OQS regime. Note that for each L_B, the time regime $t \leq t_{oqs}$ is different. Plots for larger values of L_B overlap with those of smaller values of L_B but extend to longer times. In panels (b) and (e), we fix $L_B = 26$ and consider two randomly chosen initial states (blue and yellow symbols) of the DQD. They correspond to the same two initial conditions chosen in Fig. 2. The horizontal dashed lines in panels (a), (b), (d), (e) show the corresponding expectation value obtained with the $\hat{\rho}_{MGS}$. In panels (c) and (f), we plot the trace distance between $\hat{\rho}_S(t_{oqs}; L_B)$ and $\hat{\rho}_{MGS}$ as a function of bath size L_B for the two different choices of initial states (blue and orange symbols) of the DQD. The straight lines (dashed-dotted blue and dashed red) are exponential fits to the symbols, with numerical fit parameters given. Other parameters: $g_B = 2g$, $\gamma = g$, $\beta g = 0.1$, $L_0 = 8$.

3.4 Thermalization in the IQS regime

3.4.1 Integrability breaking in the interacting DQD

Before we proceed to analyse thermalization within the IQS approach, we must distinguish between the integrable and the non-integrable case, since, as mentioned before, IQS thermalization is mainly discussed for non-integrable systems [4, 39–46, 49–61]. It has been established that a single impurity in an otherwise integrable model can make the system non-integrable [78–81]. We do a similar check for the interacting DQD, by calculating the spectral form factor (SFF) and level spacing distributions. The results are given in Appendix A. We find that the interacting DQD shows key features of non-integrability, such as level repulsion. But within the accessible values of L_B for exact diagonalization, it does not fully develop all non-integrable features. Specifically, while the level-spacing distribution deviates significantly from the Poisson distribution expected for integrable systems, it does not converge to the Wigner-Yanase distribution expected of non-integrable systems. We refer to the system's partial non-integrability behavior as non-integrable*. Uncovering these characteristics for the interacting DQD is the third result of the paper.

3.4.2 Numerical evidence for thermalization in IQS regime

The IQS regime corresponds to the dynamics of the state of the DQD on a time scale much beyond t_{oqs}. This timescale is up to $gt_{\mathrm{oqs}} \sim 10$ for $L_B = 20 \sim 26$, see Fig. 2. To explore the IQS regime, we now look at the dynamics at much longer times, up to $gt = 2000$. In Fig. 4 we plot the dynamics of one representative observable $\langle \hat{n}_1(t)\hat{n}_2(t) \rangle$, starting from a randomly chosen initial state. This plot is of the same data as in Fig. 2(a) and (c), but with the x-axis on a linear scale instead of a log-scale, and the y-axis slightly zoomed in. Panel (a) of Fig. 4 gives the dynamics in the non-interacting, or integrable case $V = 0$. It shows large oscillations which do not decrease in amplitude, even for large times and within the values of L_B considered. In panel (b) we plot the dynamics of the same observable for the interacting non-integrable* DQD model $V = g$. Now the dynamics is drastically different. While the oscillations are sizeable for small times (up to $gt \sim 400$) they are strongly suppressed beyond that time scale, persisting as smaller fluctuations. Those fluctuations decrease with increasing L_B. This long time behavior corresponds to small oscillations about a relaxed value. These results suggest that for the non-integrable* model, the dynamical behavior follows the thermalization statement of the IQS approach, showing fluctuations about a mean value which are exponentially suppressed with increase in lattice size, see Eq.(18).

Let us now explore the relaxation in the interacting DQD case in more detail, in the light of IQS thermalization, Eqs. (17), (18). We note that in Eq. (18) the time dependence of the integral up to a finite time does not play a role. So, the fluctuations (18) about a time averaged value $\overline{\langle \hat{A} \rangle}$ defined in (17) may be written as

$$\overline{\delta \langle \hat{A} \rangle^2} = \lim_{t \to \infty} \frac{1}{t} \int_0^{t_1} dt' \left| \langle \hat{A}(t') \rangle - \overline{\langle \hat{A} \rangle} \right|^2 + \lim_{t \to \infty} \frac{1}{t - t_1} \int_{t_1}^{t} dt' \left| \langle \hat{A}(t') \rangle - \overline{\langle \hat{A} \rangle} \right|^2, \qquad (37)$$

for any finite t_1. The first term on the right hand side converges to zero in the $t \to \infty$ limit, and the second term becomes identical to the infinite time average of the integrand. Therefore, explicitly neglecting the finite time behavior and defining

$$\overline{\delta \langle \hat{A} \rangle^2}(t_1, t_f) := \frac{1}{t_f - t_1} \int_{t_1}^{t_f} dt' \left| \langle \hat{A}(t') \rangle - \overline{\langle \hat{A} \rangle} \right|^2, \qquad (38)$$
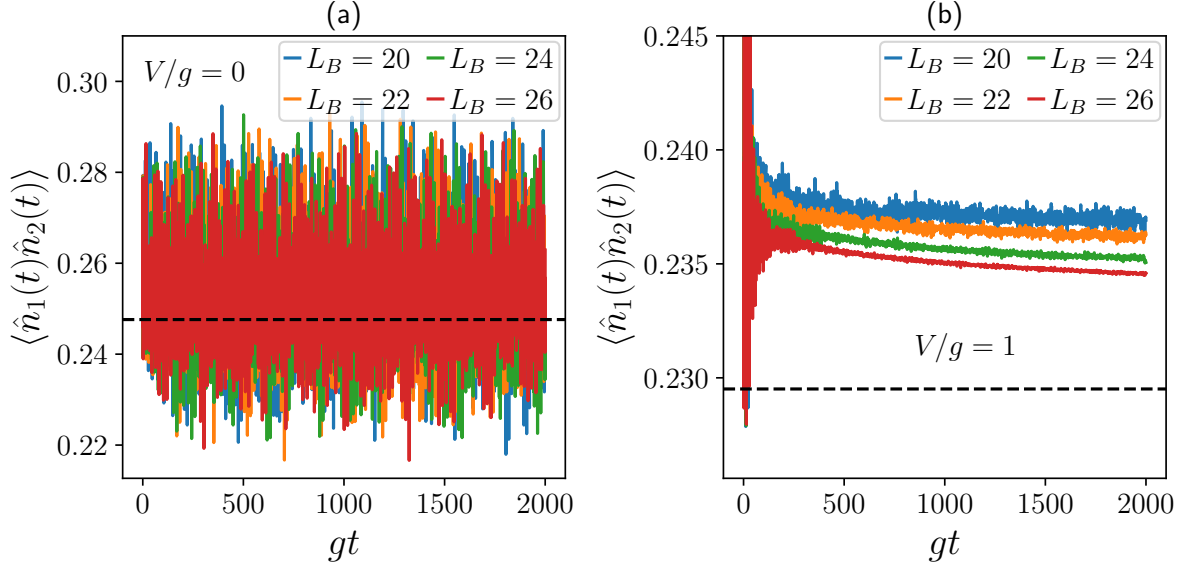
Figure 4: *Thermalization in the IQS regime:* Plot of the same data as in Fig. 2(a) and (c), only with the x-axis in linear scale instead of log-scale. In contrast to Fig. 3, where we considered maximal times up to $gt_{\text{oqs}} \sim 5 - 8$, we now consider the whole time range of gt up to 2000. The horizontal dashed lines in panels (a) and (b) show the corresponding expectation value obtained with $\hat{\rho}_{\text{MGS}}$. Panel (a) shows the free, integrable, DQD case $V = 0$. Oscillations are found to persist for all times and for all the chosen values of L_B. Panel (b) shows the dynamics in the interacting, non-integrable* case $V = g$. The large oscillations disappear after some time $gt \sim 400$ and only small fluctuations about a relaxed value persist. Those small fluctuations diminish rapidly with increasing bath size L_B. Other parameters: $\beta g = 0.1$, $\gamma = g$, $g_B = 2g$.

the exponential decay of fluctuations, Eq. (18), can be re-written as

$$\lim_{t_f \to \infty} \overline{\delta \langle \hat{A} \rangle^2}(t_1, t_f) \leq C \, e^{-\alpha L_B}, \quad \forall \, t_1 \geq t^*(L_B). \tag{39}$$

Here C and α take numerical values specific to the observable $\hat{A}$, while being independent of bath size L_B. So, the above expression says that there exists a time $t^*(L_B)$, beyond which the variance of values of $\langle \hat{A}(t) \rangle$ is exponentially small in bath size L_B. Our plots in Fig. 4 show that no such time exists for the non-interacting DQD. In contrast, the plots of the interacting DQD show that after some large fluctuations for a short initial time, the variance quickly reduces and remaining oscillations diminish with increasing bath sizes.

We now establish this more clearly for the interacting DQD with $V = g$. For numerical simplicity, we approximate $\overline{\delta \langle \hat{A} \rangle^2}(t_1, t_f)$ by the variance of data points when calculating $\langle \hat{A}(t) \rangle$ over the time range from t_1 to t_f. For the interacting DQD, we now plot in Fig. 5(a) the numerical value of the variance $\overline{\delta \langle \hat{n}_1 \hat{n}_2 \rangle^2}(t_1, t_f)$ for fixed $t_f = 2000g^{-1}$, as a function of initial time t_1, and for various values of L_B (varying colours). The variance initially decays exponentially with t_1. For late times $t_1 > t^*(L_B)$, some time $t^*(L_B)$, the value of $\overline{\delta \langle \hat{A} \rangle^2}(t_1, t_f)$ settles to an approximately constant value, which we denote by $v(L_B)$. The value of $t^*(L_B)$ increases with L_B. This, once again, highlights the importance of taking $t \to \infty$ first in Eq. (18).

We also see that the value $v(L_B)$ decreases exponentially with L_B, i.e. it obeys the bound $v(L_B) \lesssim C \, e^{-\alpha L_B}$. This is evident from the log-plot shown in Fig. 5(a). To establish this more clearly, we plot the long-time constant values $v(L_B)$ for all four operators of the DQD (see Eq. (25)) as a function of L_B in Fig. 5(b). We see that all these quantities decay exponentially
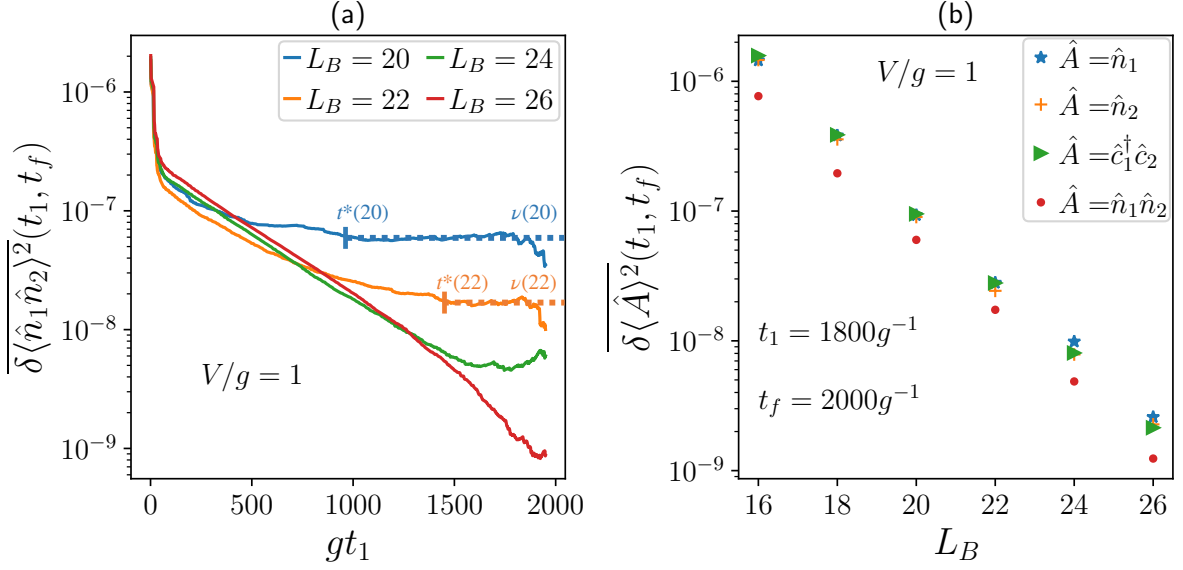
Figure 5: *IQS thermalization of interacting DQD with variable bath size L_B*: (a) Log-plot of the variance $\overline{\delta\langle\hat{n}_1\hat{n}_2\rangle^2}(t_1,t_f)$ of data points shown in Fig. 4(b), as a function of initial interval time t_1, while keeping the final interval time fixed, $gt_f = 2000$. Here t_1 is varied between $0 \leq t_1 \leq 1900g^{-1}$. Different colours indicate results for various bath sizes L_B. After a time $t^*(L_B)$, the dynamics reaches an approximately constant value which we call $v(L_B)$ (horizontal dashed lines). The spacing between these saturation values is equal as L_B varies over the values $L_B = 20, 22, 24, 26$, which indicates exponential decay of $v(L_B)$ with L_B. (b) Log-plot of the long-time variance $\overline{\delta\langle\hat{A}\rangle^2}(t_1,t_f)$ for each of the four observables $\hat{A}$ of the interacting DQD, as a function of L_B. The times t_1, t_f are taken large, so that the variance has reached the approximately constant value (c.f. panel (a)). The quantities $\overline{\delta\langle\hat{A}\rangle^2}(t_1,t_f)$ are numerically evaluated via Eq. (38) with $t_1 = 1800g^{-1}$ and $t_f = 2000g^{-1}$. The plots show that the variance of each observable $\hat{A}$ decays exponentially with L_B, in line with Eq. (39). Other parameters: $V = g, \beta g = 0.1, \gamma = g, g_B = 2g$.

with L_B. These observations numerically evidence the exponential decay of the variance with L_B required for IQS thermalization, see Eqs. (39) and (18).

In order to check numerically the validity of Eq. (19), we define for any operator $\hat{A}$,

$$\mathcal{E}\left(\overline{\langle\hat{A}\rangle}\right) = \left|\frac{\overline{\langle\hat{A}\rangle} - A_{\mathrm{MGS}}}{A_{\mathrm{MGS}}}\right|. \tag{40}$$

This measures the deviation of the expectation from its value in the mean force Gibs state, see (20). From (19) we expect $\mathcal{E}\left(\overline{\langle\hat{A}\rangle}\right) = d/L_B + f$ with d specific to the observable $\hat{A}$ while independent of L_B, and an offset f which should be negligible. In Fig. 6(a), we now plot $\mathcal{E}\left(\overline{\langle\hat{A}\rangle}\right)$, as a function of $1/L_B$, for all four system operators (25). Here the time average is taken over the same range as in Fig. 5(b). (Note that we have also verified that this plot is almost unaffected by choosing a much smaller value of t_1, as long as $t_1 \gg t_{\mathrm{oqs}}$.) We clearly see that $\mathcal{E}\left(\overline{\langle\hat{A}\rangle}\right)$ decays linearly as $1/L_B$ for all choices of $\hat{A}$, with a small offset f (y-intercept).

To see this more generally, we plot in Fig. 6(b) the trace distance between the time averaged density matrix $\overline{\hat{\rho}} := \frac{1}{t_f - t_i}\int_{t_i}^{t_f} dt'\hat{\rho}(t')$ of the DQD, and the state $\hat{\rho}_{\mathrm{MGS}}$, as a function of $1/L_B$. This is done for three different randomly chosen initial conditions of the DQD. We again clearly
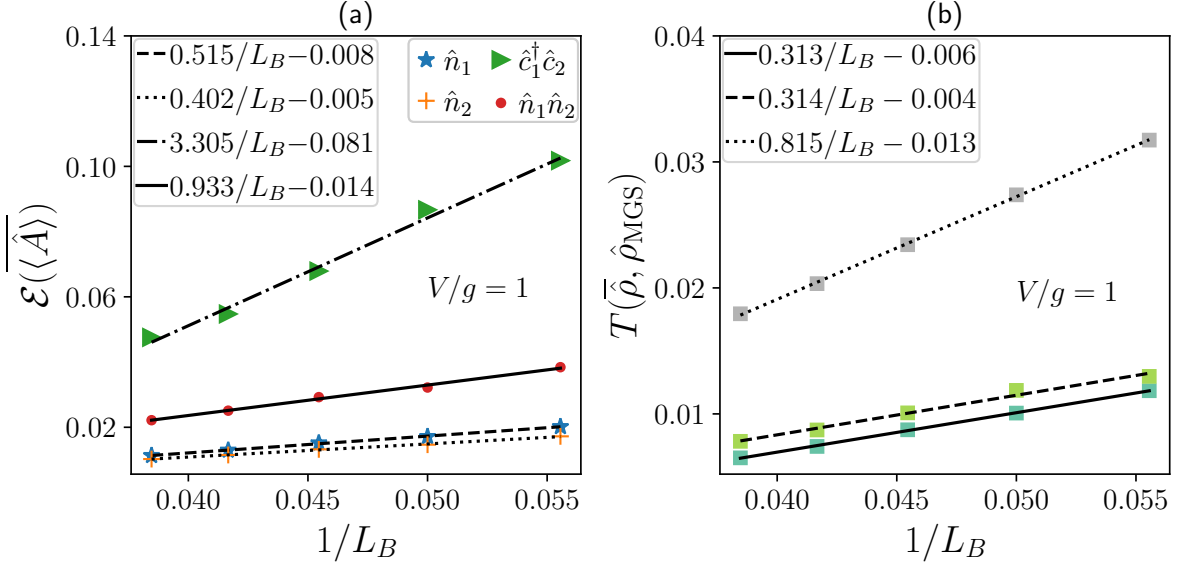
Figure 6: *Decaying deviations from full thermalization in the IQS regime*: (a) Relative deviation $\mathcal{E}\left(\overline{\langle \hat{A} \rangle}\right)$, see Eq. (40), of operator expectation values from their mean force Gibbs state (thermal) values as function of $1/L_B$, for all four DQD operators. Linear fits (dashed, dotted, dash-dotted, solid) show excellent consistency with (19), for all four operators (25). (b) Trace distance T between the time averaged density matrix $\overline{\hat{\rho}}$ and the mean force Gibbs state $\hat{\rho}_{\mathrm{MGS}}$ as a function of $1/L_B$, for three randomly chosen initial states of the DQD (gray, light green, dark green squares). Linear fits (dotted, dashed, solid) show excellent consistency with (19), for all three initial states drawn from (29). Other parameters: $\beta g = 0.1$, $\gamma = g$, $g_B = 2g$. Time averages are taken between t_1 and t_f as chosen in Fig. 5(b).

see a $1/L_B$ decay with a small offset in all cases. Neglecting the small offset, this is completely consistent with Eq. (19). We attribute this small spurious offset to numerical limitations [see Appendix. B].

Combining all of the above, we see that the interacting DQD, satisfies Eqs. (18) and (19), and therefore shows thermalization in the IQS sense for $t \gg t_{\mathrm{oqs}}$. In contrast, the non-interacting DQD does not thermalize in the IQS sense, at least within the range of time and L_B considered. Our numerical results clearly highlight that for thermalization in the IQS sense to hold, we need to first take the long time limit in Eqs. (17) and (18) for a fixed bath size L_B, before considering increased bath sizes. This is the fourth result of the paper.

4 Summary and outlook

In this work we have carried out a systematic comparison between the notions and conditions of thermalization in OQS and IQS, on the basis of a model consisting of a DQD coupled to a fermionic lead. The notion of thermalization involves taking both the long time and the thermodynamic limits. We show that both the OQS and the IQS approach investigate the convergence to the same state. However, they apply the two limits in a different order: while in the OQS one first performs the thermodynamic limit and then the long-time limit, it is the other way around in the IQS approach. As a consequence, the two approaches give the convergence to the final state at markedly different timescales. This timescale separation in the

two thermalization notions, to our knowledge, is a new insight. We believe it stems from the fact that in the IQS approach, the system and the environment are considered a single complex, and relaxation to equilibrium is required at all locations within this complex. In contrast, in the OQS approach, only local variables of the system alone, and not those of the environment, are required to show thermalization, resulting in a faster process.

Using the concept of typicality, we have constructed the class of initial states usually considered in the OQS approach, as a special type of randomly chosen pure state. This class of states allows the initial state of the DQD to be arbitrary while the reduced bath state is thermal, and allows to study both notions of thermalization on an equal footing. Our main finding is that the dynamics starting from such a state shows a clear crossover between OQS and IQS behavior. The OQS regime corresponds to the time scale t_{oqs} within which the system hardly feels the finite size of the bath. Lieb-Robinson bounds can be invoked to show that t_{oqs} is roughly proportional to bath size L_B for large L_B. Regardless of the initial state of the DQD, the state of the DQD at time t_{oqs} converges to the mean-force Gibbs state $\hat{\rho}_{\mathrm{MGS}}$ as L_B is increased. This corresponds to thermalization in the OQS sense and it holds irrespective of the presence of many-body interactions within the DQD. Note that, although expected, to our knowledge, the convergence of OQS dynamics to $\hat{\rho}_{\mathrm{MGS}}$ has not been previously numerically demonstrated for any system with many-body interactions.

We then showed that thermalization in the IQS sense takes place at times $t \gg t_{\mathrm{oqs}}$. In this regime, the DQD is affected by the finiteness of the bath. In this sense, the dynamics of the DQD may no longer be considered as that of an open system and one is led to view the DQD plus the environment as a single, isolated system. It is known that integrable Hamiltonians do not thermalize in this regime, but according to ETH considerations, non-integrable ones are expected to. The free DQD case corresponds to free fermions, thereby is integrable and is not expected to thermalize in this regime, which we confirmed via numerical investigation.

In contrast, for the interacting DQD, we found that the presence of many-body interaction within the DQD breaks integrability. This was evidenced by the shape of the spectral form factor and the system's level spacing statistics. At the numerically accessible values of L_B, while we found clear signature of level-repulsion which is a hallmark of non-integrable behavior, we did not fully recover the expected Wigner-Dyson distribution. This non-integrable* behavior could be a finite-size effect, and full convergence could still manifest at increasing L_B. Regardless of the only partially non-integrable character of the interacting DQD within our accessible values of L_B, we found strong evidence of IQS thermalization at times $t \gg t_{\mathrm{oqs}}$.

Our results open several directions for further research. While here we focused on the behavior of observables defined locally on the reduced system (i.e., the DQD), it will be extremely interesting to extend the analysis to observables defined locally on the bath. Our approach could be applied to other fermionic models than the one investigated here. Here, the Hamiltonian parameters in the DQD are different from the lead, allowing a natural separation between system and bath. However, the same protocol can be applied to a situation with uniform Hamiltonian parameters, thereby having no natural separation, providing an interesting avenue for future work. In this connection, free fermionic models would also be of interest [82–85]. Overall, we believe our results call for a more in-depth study of the necessary assumptions for IQS thermalization, as well as, a systematic comparison of OQS/IQS thermalization in a broader class of models.

5　Acknowledgements

A   Appendix: Numerical results for integrability breaking in the interacting DQD

We check the integrability of our model using the spectral form factor (SFF), as well as the level-spacing distribution. In order to do so, we restrict ourselves to the half-filled sector of the full Hamiltonian, whose dimension, we denote by D. The SFF is defined as

$$\text{SFF} = \frac{1}{D^2} \left| \text{Tr}(e^{-i\hat{H}t}) \right|^2. \tag{41}$$

It is known [86–95], that for non-integrable systems the SFF shows a characteristic dip, ramp and plateau behavior as a function of t. The ramp and plateau expression has the form $b_2(Wt/(2\pi D))$, where $W = E_{max} - E_{min}$ is the difference between largest and smallest eigenvalue of $\hat{H}$ and the function b_2 is

$$b_2(x) = \frac{1}{D} \left[1 - [1 - 2x + x\log(2x+1)] \, \Theta(1-x) + \left[x\log\left(\frac{2x+1}{2x-1}\right) - 1 \right] \Theta(x-1) \right], \tag{42}$$

with $\Theta(x)$ being the Heaviside step function. At $x = 1$ the function switches from an approximately linear ramp, to an approximately constant plateau with the value $1/D$. For integrable systems, this universal ramp and plateau behavior will be missing.

We numerically evaluate the SFF for both the non-interacting DQD case and the interacting DQD case. The plots of the SFF are shown in blue in Fig. 7. It is clear that the non-interacting DQD case does not show any resemblance to b_2 (orange) even at long times. However, the interacting DQD case with $V = g$ indeed shows a ramp and plateau which resembles the universal function b_2. This provides numerical evidence that the interacting DQD case has non-integrable features.

Integrable vs. chaotic behavior can also be assessed by analysing the energetic spectra [50]. For example, the spectra for transmon qubit gates have been found to show chaotic fluctuations [96]. Here we follow this approach and calculate the energetic level spacing distribution for the full Hamiltonian in the half-filled sector. Let us write the full Hamiltonian as $\hat{H} = \sum_{\alpha=1}^{D} E_\alpha |E_\alpha\rangle \langle E_\alpha|$, where E_α are the energy eigenvalues, arranged in ascending order of energy, $|E_\alpha\rangle$ are the corresponding energy eigenvectors, and d is the dimension of the half-filled Hilbert space. The level-spacing distribution is given by

$$P(s) = \frac{1}{\mathcal{N}} \sum_{\alpha=1}^{D-1} \delta\left(s - \frac{E_{\alpha+1} - E_\alpha}{\Delta} \right), \tag{43}$$
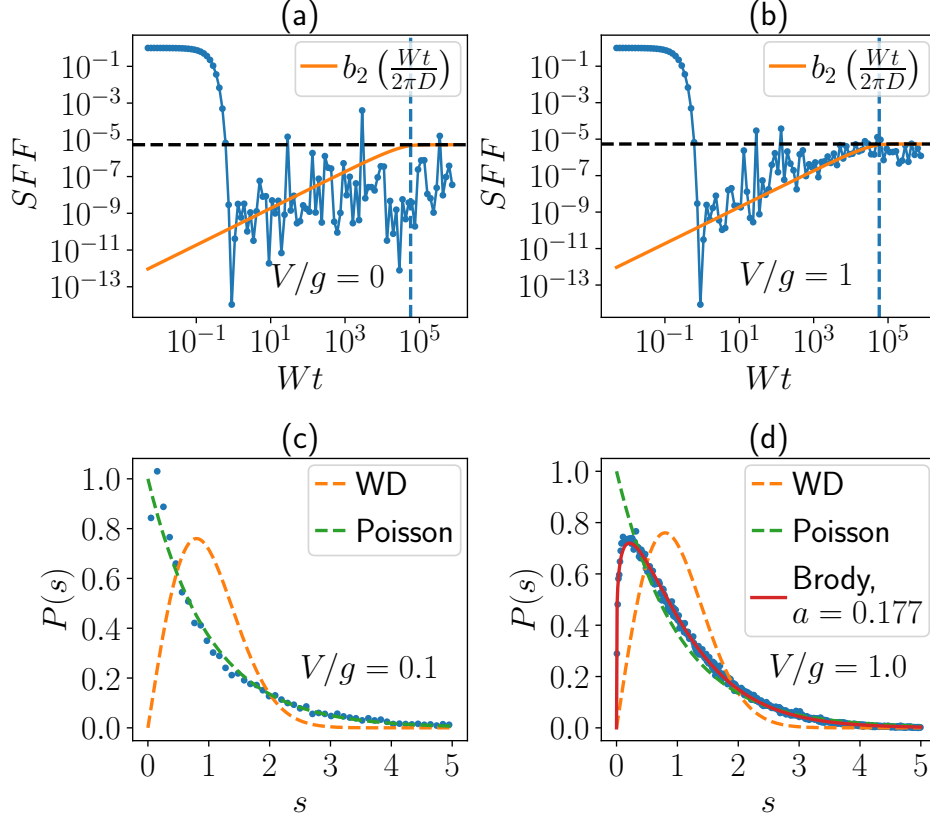
Figure 7: *Checking integrability of the interacting DQD:* The spectral form factor (SFF) (41) of the full Hamiltonian $\hat{H}$ in (1) is plotted (blue symbols) as a function of Wt, with $W = E_{max} - E_{min}$, for the non-interacting DQD case $V = 0$ in panel (a), and for the interacting DQD case with $V/g = 1$ in panel (b). The function b_2 (orange line) is the universal expression given in Eq. (42). The SFF in panel (a) does not approach the function b_2, while in panel (b), after an initial dip, the SFF oscillates around b_2, evidencing the SFF behavior expected of a non-integrable model. The vertical dashed line shows the transition point from ramp to plateau, at $Wt = 2\pi D$, with $D = 2^{L_B+2}$. The results in (a) and (b) are for $L_B = 18$ (total chain size $L_B + 2 = 20$). The horizontal dashed line is located at $1/D$. Panel (c) shows the system's level-spacing distribution $P(s)$ (blue dots) at $V/g = 0.1$ (almost free fermion case) for $L_B = 18$. It is evident that it is close to the Poissonian distribution $P^{\text{Poi}}(s)$, (44) (dashed green), as expected for an integrable system. Panel (d) shows the level distribution $P(s)$ for the interacting DQD model at $V/g = 1.0$ for $L_B = 18$. The level-spacing distribution is still far from the Wigner-Dyson (WD) distribution (dashed yellow) expected for fully non-integrable systems. But, $P(s)$ closely follows a Brody distribution (red line) which, unlike the Poisson distribution (dashed green), goes to zero at zero spacing s.

where Δ is the mean 'local' nearest neighbour level spacing, $\mathcal{N}$ is a normalization constant, and $\delta(x)$ is the Dirac delta function. For integrable systems, a large number of degeneracies of energy levels is expected. The corresponding level spacing distribution is Poissonian [47, 48, 50, 81]

$$P^{\text{Poi}}(s) \propto e^{-s} \qquad \text{(for integrable systems)}. \qquad (44)$$

For non-integrable systems, no degeneracy of energy levels within a symmetry sector is expected. This is termed level-repulsion. In fact, if our system is fully non-integrable, the level-spacing distribution is expected to correspond to that of a random matrix of the Gaussian orthogonal
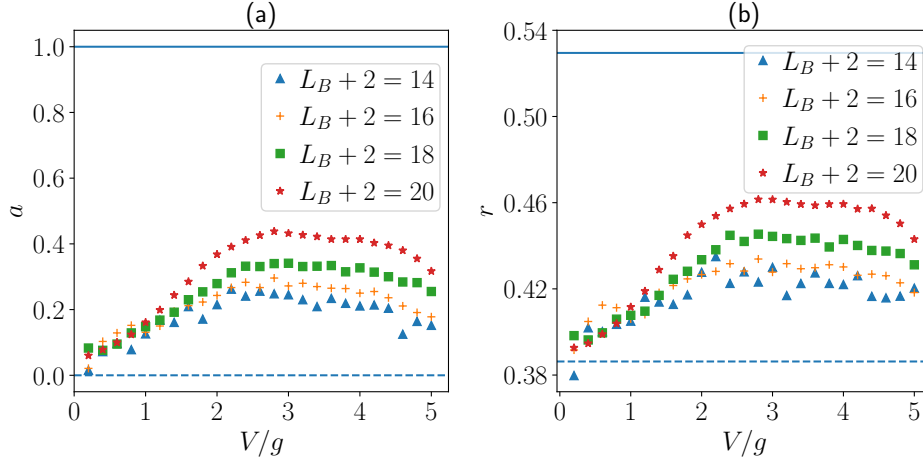
Figure 8:   *Non-integrability of the interacting DQD:* (a) The figure shows the values of a, obtained by fitting the level-spacing distribution at half filling ($N = \frac{L_B}{2} + 1$) of the interaction DQD with the Brody distribution, as a function of interaction strength V, for various values of L_B (chain length is $L_B + 2$). The value $a = 0$ (dashed horizontal line) corresponds to a Poisson distribution, which is expected for integrable systems, while $a = 1$ (continuous horizontal line) corresponds to a Wigner-Dyson distribution, expected for fully non-integrable systems. (b) The figure shows the values of r, which is the mean ratio of successive energy gaps, as a function of V for various values of L_B. The dashed horizontal line corresponds to $r = 2\ln 2 - 1 \approx 0.3863$, which is expected for Poisson distribution, while the continuous horizontal line corresponds to $r = 0.5295$, which approximates the expected value for Wigner-Dyson distribution.

ensemble (GOE), which is called the Wigner-Dyson (WD) distribution [47, 48, 50, 81],

$$P^{\text{WD}}(s) = \frac{\pi s}{2} e^{-\pi s^2/4} \qquad \text{(for fully non-integrable systems).} \tag{45}$$

There is another distribution called the Brody distribution that smoothly interpolates between the Poisson distribution and the WD distribution [47, 48, 81],

$$P^{\text{Bro}}(s) = (a+1)\, b\, s\, e^{-b\, s^{(a+1)}} \quad 0 \le a \le 1 \quad \text{(for partially non-integrable systems),} \tag{46}$$

where $b = \Gamma\left(\frac{a+1}{a+1}\right)^{a+1}$. For $a = 0$, the Brody distribution becomes the Poisson distribution, while for $a = 1$, it becomes the WD distribution. Importantly, the Brody distribution for $a > 0$ also goes to zero at $s = 0$, signifying level repulsion.

Calculating the level-spacing distribution requires unfolding of the spectrum. To achieve this, in our calculation, for each α, we divide the spacing by a rolling average over a chosen window size around that energy. Additionally, around 1% of eigenvalues from the top and the bottom of the spectrum are neglected. Although often not explicitly written in most recent works, these are rather standard procedures to obtain the level-spacing distribution.

To ensure that there is no particular artefact stemming from the above unfolding procedure, we also consider the ratio of adjacent gaps, defined as

$$r_\alpha = \frac{\min(E_{\alpha+1} - E_\alpha, E_\alpha - E_{\alpha-1})}{\max(E_{\alpha+1} - E_\alpha, E_\alpha - E_{\alpha-1})}. \tag{47}$$

Let r be the mean value of r_α, averaged over all α. The value of r is known for cases when the spacing distribution matches Poisson and WD distributions, i.e., for integrable and non-integrable systems: $r = 2\ln 2 - 1$ for integrable systems, and $r \approx 0.5295$ for non-integrable

systems. The value of r is also routinely used to characterize integrability-breaking in quantum systems. Unlike the level-spacing distribution calculating this quantity does not require unfolding of the spectrum.

The spacing distribution for our system is shown in Figs. 7(c) and (d). In Fig. 7(c), we show the spacing distribution for a small value of V/g. For such small values of V/g, at accessible system sizes, the distribution is close to $P^{\mathrm{Poi}}(s)$. However, on increasing V/g, the level repulsion becomes clear, and the distribution fits very well to a Brody distribution with $0 < a < 1$. This is shown for $V/g = 1$ in Fig. 7(d). In Fig. 8(a), we plot the fitted Brody-distribution parameter a versus the interaction strength, for various system sizes. We find that the WD distribution corresponding to $a \to 1$ is not recovered even for larger values of V/g. However, the value of a does increase with increase in chain length, up to a value of ca. $a \approx 0.45$. A similar approach towards markers of non-integrability is seen in the mean ratio of adjacent gaps, r. The value of r remains in between that expected for integrable and fully non-integrable systems. But r also seems to increase towards the non-integrable value on increasing chain length. From these numerical results, it seems that at the numerically accessible chain lengths, the system would be neither integrable nor fully non-integrable. We call such finite-size systems 'partially non-integrable', denoted in short as non-integrable*. It is crucial to note that, level-repulsion, which is a key aspect of non-integrable systems, is already clear even at such finite chain lengths. On further increasing chain lengths, the spacing distribution may recover the full WD form, but we leave confirmation of this for future research.

B Appendix: Numerical limitations for results of dynamics

Although the numerical technique we have used is quite powerful and has allowed us to simulate quite large chain lengths up to considerably long times, there are certain limitations, which can lead to small errors that are hard to reduce. We believe the small spurious offset seen in linear fits of Fig. 6 stem from these errors. Here, we describe the main possible sources of such errors.

First, we used a single typical state to approximate a thermal state. This is done both for the initial condition, and in calculating the expectation values corresponding to $\hat{\rho}_{\mathrm{MGS}}$. While this is a good approximation at large enough system sizes, this is not exact and small sample to sample fluctuations are expected at any finite system size. Deviations between expectation values obtained from a single typical state and those from a thermal state may be reduced by ensemble averaging. But, although they reduce exponentially with system size, for a given system size, they are not expected to decrease as fast with ensemble averaging. Therefore, reducing the deviations at a given system size require averaging over a large number of samples. Since we are performing a long time simulation (up to $t = 2000g^{-1}$), with quite large many-body systems (up to total chain length is 28 sites, size of the largest block of Hamiltonian in Fock space is of size 40116600), using a single typical state is already computationally quite expensive. This makes taking average over a large number of typical states impractical. So, at present, we are unable to make a systematic check of whether the offset can be reduced via ensemble averaging.

Second, in Figs. 4(b), it is apparent that, although there is relaxation, the simulation might not have reached the asymptotic value within the time range considered. It may be that taking time averages over much larger time regimes reduces the offset. This is again hard to check, because going to longer times is also expensive. However, within our time regime, we have seen that taking time average over any time regime with $t_1 \gg t_{\mathrm{oqs}}$ yields plots similar to Figs. 6 with quantitatively similar offsets.

Third, our numerical data is taken in steps of time $gt = 1$. Taking such large time steps is one of the advantages of the Chebyshev polynomial method that we utilize to make such long time simulations tractable within our computational resources. This, however, also means that

the average of data points deviates from the actual time average defined in terms of an integral. So, it may be that the spurious offset can be reduced on taking a finer time-grid. But, this again, would increase simulation time greatly, making the simulation impractical.

References

[1] J. M. Deutsch, *Quantum statistical mechanics in a closed system*, Phys. Rev. A **43**, 2046 (1991), doi:10.1103/PhysRevA.43.2046.

[2] M. Srednicki, *Chaos and quantum thermalization*, Phys. Rev. E **50**, 888 (1994), doi:10.1103/PhysRevE.50.888.

[3] M. Srednicki, *The approach to thermal equilibrium in quantized chaotic systems*, Journal of Physics A: Mathematical and General **32**(7), 1163 (1999), doi:10.1088/0305-4470/32/7/007.

[4] M. Rigol, V. Dunjko and M. Olshanii, *Thermalization and its mechanism for generic isolated quantum systems*, Nature **452**(7189), 854 (2008), doi:10.1038/nature06838.

[5] S. Goldstein, J. L. Lebowitz, C. Mastrodonato, R. Tumulka and N. Zanghì, *Normal typicality and von neumann's quantum ergodic theorem*, Proceedings of the Royal Society A: Mathematical, Physical and Engineering Sciences **466**(2123), 3203 (2010), doi:10.1098/rspa.2009.0635.

[6] B. Buča, *Unified theory of local quantum many-body dynamics: Eigenoperator thermalization theorems*, Phys. Rev. X **13**, 031013 (2023), doi:10.1103/PhysRevX.13.031013.

[7] A. S. Trushechkin, M. Merkli, J. D. Cresser and J. Anders, *Open quantum system dynamics and the mean force Gibbs state*, AVS Quantum Science **4**(1), 012301 (2022), doi:10.1116/5.0073853.

[8] J. D. Cresser and J. Anders, *Weak and ultrastrong coupling limits of the quantum mean force gibbs state*, Phys. Rev. Lett. **127**, 250601 (2021), doi:10.1103/PhysRevLett.127.250601.

[9] J. Thingna, J.-S. Wang and P. Hänggi, *Generalized gibbs state with modified redfield solution: Exact agreement up to second order*, The Journal of Chemical Physics **136**(19), 194110 (2012), doi:10.1063/1.4718706.

[10] Y. Subaş ı, C. H. Fleming, J. M. Taylor and B. L. Hu, *Equilibrium states of open quantum systems in the strong coupling regime*, Phys. Rev. E **86**, 061132 (2012), doi:10.1103/PhysRevE.86.061132.

[11] A. Dhar, K. Saito and P. Hänggi, *Nonequilibrium density-matrix description of steady-state quantum transport*, Phys. Rev. E **85**, 011126 (2012), doi:10.1103/PhysRevE.85.011126.

[12] A. Dhar and D. Sen, *Nonequilibrium green's function formalism and the problem of bound states*, Phys. Rev. B **73**, 085119 (2006), doi:10.1103/PhysRevB.73.085119.

[13] D. Roy and A. Dhar, *Heat transport in ordered harmonic lattices*, Journal of Statistical Physics **131**(3), 535 (2008), doi:10.1007/s10955-008-9487-1.

[14] E. B. Davies, *Markovian master equations*, Commun. Math. Phys. **39**, 91 (1974), doi:10.1007/BF01608389.

[15] E. B. Davies, *Markovian master equations. II.*, Math. Ann. **219**, 147–158 (1976), doi:10.1007/BF01351898.

[16] V. Jaksic and C.-A. Pillet, *On a model for quantum friction III. Ergodic properties of the spin-boson system*, Commun. Math. Phys **178**, 627 (1996), doi:10.1063/1.533334.

[17] V. Bach, J. Fröhlich and I. Sigal, *Return to equilibrium*, Journal of Mathematical Physics **41(6)**, 3985 (2000), doi:10.1063/1.533334.

[18] M. Merkli, I. M. Sigal and G. P. Berman, *Decoherence and thermalization*, Phys. Rev. Lett. **98**, 130401 (2007), doi:10.1103/PhysRevLett.98.130401.

[19] M. Merkli, *Quantum markovian master equations: Resonance theory shows validity for all time scales*, Annals of Physics **412**, 167996 (2020), doi:https://doi.org/10.1016/j.aop.2019.167996.

[20] M. Merkli, *Dynamics of Open Quantum Systems II, Markovian Approximation*, Quantum **6**, 616 (2022), doi:10.22331/q-2022-01-03-616.

[21] M. Merkli, *Dynamics of Open Quantum Systems I, Oscillation and Decay*, Quantum **6**, 615 (2022), doi:10.22331/q-2022-01-03-615.

[22] M. Merkli, *Correlation decay and markovianity in open systems*, Ann. Henri Poincaré **24**, 751 (2023), doi:10.1007/s00023-022-01226-5.

[23] H.-P. Breuer and F. Petruccione, *The Theory of Open Quantum Systems*, Oxford University Press, Oxford, doi:10.1093/acprof:oso/9780199213900.001.0001 (2007).

[24] A. Rivas and S. F. Huelga, *Open Quantum Systems*, Springer Berlin Heidelberg, ISBN 9783642233548, doi:10.1007/978-3-642-23354-8 (2012).

[25] H. Haug and A.-P. Jauho, *Quantum Kinetics in Transport and Optics of Semiconductors*, Springer-Verlag Berlin Heidelberg, doi:10.1007/978-3-540-73564-9 (2008).

[26] A. Kamenev, *Field Theory of Non-Equilibrium Systems*, Cambridge University Press, Cambridge, doi:10.1017/CBO9781139003667 (2011).

[27] J.-S. Wang, B. K. Agarwalla, H. Li and J. Thingna, *Nonequilibrium green's function method for quantum thermal transport*, Frontiers of Physics **9(6)**, 673 (2014), doi:10.1007/s11467-013-0340-x.

[28] C. Gardiner and P. Zoller, *Quantum Noise*, Springer-Verlag Berlin, Heidelberg (2004).

[29] E. Cortés, B. J. West and K. Lindenberg, *On the generalized langevin equation: Classical and quantum mechanicala)*, The Journal of Chemical Physics **82**(6), 2708 (1985), doi:10.1063/1.448268.

[30] R. Benguria and M. Kac, *Quantum langevin equation*, Phys. Rev. Lett. **46**, 1 (1981), doi:10.1103/PhysRevLett.46.1.

[31] G. W. Ford, J. T. Lewis and R. F. O'Connell, *Quantum langevin equation*, Phys. Rev. A **37**, 4419 (1988), doi:10.1103/PhysRevA.37.4419.

[32] A. Dhar and B. Sriram Shastry, *Quantum transport using the ford-kac-mazur formalism*, Phys. Rev. B **67**, 195405 (2003), doi:10.1103/PhysRevB.67.195405.

[33] P. Talkner and P. Hänggi, *Colloquium: Statistical mechanics and thermodynamics at strong coupling: Quantum and classical*, Rev. Mod. Phys. **92**, 041002 (2020), doi:10.1103/RevModPhys.92.041002.

[34] A. Rivas, *Strong coupling thermodynamics of open quantum systems*, Phys. Rev. Lett. **124**, 160601 (2020), doi:10.1103/PhysRevLett.124.160601.

[35] W.-M. Huang and W.-M. Zhang, *Nonperturbative renormalization of quantum thermodynamics from weak to strong couplings*, Phys. Rev. Res. **4**, 023141 (2022), doi:10.1103/PhysRevResearch.4.023141.

[36] D. Tupkary, A. Dhar, M. Kulkarni and A. Purkayastha, *Fundamental limitations in lindblad descriptions of systems weakly coupled to baths*, Phys. Rev. A **105**, 032208 (2022), doi:10.1103/PhysRevA.105.032208.

[37] D. Tupkary, A. Dhar, M. Kulkarni and A. Purkayastha, *Searching for lindbladians obeying local conservation laws and showing thermalization*, Phys. Rev. A **107**, 062216 (2023), doi:10.1103/PhysRevA.107.062216.

[38] T. Becker, A. Schnell and J. Thingna, *Canonically consistent quantum master equation*, Phys. Rev. Lett. **129**, 200403 (2022), doi:10.1103/PhysRevLett.129.200403.

[39] H. Tasaki, *From quantum dynamics to the canonical distribution: General picture and a rigorous example*, Phys. Rev. Lett. **80**, 1373 (1998), doi:10.1103/PhysRevLett.80.1373.

[40] P. Reimann, *Foundation of statistical mechanics under experimentally realistic conditions*, Phys. Rev. Lett. **101**, 190403 (2008), doi:10.1103/PhysRevLett.101.190403.

[41] N. Linden, S. Popescu, A. J. Short and A. Winter, *Quantum mechanical evolution towards thermal equilibrium*, Phys. Rev. E **79**, 061103 (2009), doi:10.1103/PhysRevE.79.061103.

[42] P. Reimann, *Canonical thermalization*, New Journal of Physics **12**(5), 055027 (2010), doi:10.1088/1367-2630/12/5/055027.

[43] V. I. Yukalov, *Equilibration and thermalization in finite quantum systems*, Laser Physics Letters **8**(7), 485 (2011), doi:10.1002/lapl.201110002.

[44] A. Polkovnikov, K. Sengupta, A. Silva and M. Vengalattore, *Colloquium: Nonequilibrium dynamics of closed interacting quantum systems*, Rev. Mod. Phys. **83**, 863 (2011), doi:10.1103/RevModPhys.83.863.

[45] P. Reimann and M. Kastner, *Equilibration of isolated macroscopic quantum systems*, New Journal of Physics **14**(4), 043020 (2012), doi:10.1088/1367-2630/14/4/043020.

[46] A. J. Short and T. C. Farrelly, *Quantum equilibration in finite time*, New Journal of Physics **14**(1), 013063 (2012), doi:10.1088/1367-2630/14/1/013063.

[47] R. Modak and S. Mukerjee, *Finite size scaling in crossover among different random matrix ensembles in microscopic lattice models*, New Journal of Physics **16**(9), 093016 (2014), doi:10.1088/1367-2630/16/9/093016.

[48] R. Modak, S. Mukerjee and S. Ramaswamy, *Universal power law in crossover from integrability to quantum chaos*, Phys. Rev. B **90**, 075152 (2014), doi:10.1103/PhysRevB.90.075152.

[49] P. Reimann, *Eigenstate thermalization: Deutsch's approach and beyond*, New Journal of Physics **17**(5), 055025 (2015), doi:10.1088/1367-2630/17/5/055025.

[50] L. D'Alessio, Y. Kafri, A. Polkovnikov and M. Rigol, *From quantum chaos and eigenstate thermalization to statistical mechanics and thermodynamics*, Advances in Physics **65**(3), 239 (2016), doi:10.1080/00018732.2016.1198134.

[51] P. Reimann, *Typical fast thermalization processes in closed many-body systems*, Nature Communications **7**(1), 10821 (2016), doi:10.1038/ncomms10821.

[52] M. Rigol, *Fundamental asymmetry in quenches between integrable and nonintegrable systems*, Phys. Rev. Lett. **116**, 100601 (2016), doi:10.1103/PhysRevLett.116.100601.

[53] C. Gogolin and J. Eisert, *Equilibration, thermalisation, and the emergence of statistical mechanics in closed quantum systems*, Reports on Progress in Physics **79**(5), 056001 (2016), doi:10.1088/0034-4885/79/5/056001.

[54] T. Farrelly, F. G. S. L. Brandão and M. Cramer, *Thermalization and return to equilibrium on finite quantum lattice systems*, Phys. Rev. Lett. **118**, 140601 (2017), doi:10.1103/PhysRevLett.118.140601.

[55] C. Bartsch and J. Gemmer, *Necessity of eigenstate thermalisation for equilibration towards unique expectation values when starting from generic initial states*, Europhysics Letters **118**(1), 10006 (2017), doi:10.1209/0295-5075/118/10006.

[56] T. R. de Oliveira, C. Charalambous, D. Jonathan, M. Lewenstein and A. Riera, *Equilibration time scales in closed many-body quantum systems*, New Journal of Physics **20**(3), 033032 (2018), doi:10.1088/1367-2630/aab03b.

[57] J. Eisert, M. Friesdorf and C. Gogolin, *Quantum many-body systems out of equilibrium*, Nature Physics **11**(2), 124 (2015), doi:10.1038/nphys3215.

[58] R. Steinigeweg, J. Herbrych and P. Prelovšek, *Eigenstate thermalization within isolated spin-chain systems*, Phys. Rev. E **87**, 012118 (2013), doi:10.1103/PhysRevE.87.012118.

[59] G. De Palma, A. Serafini, V. Giovannetti and M. Cramer, *Necessity of eigenstate thermalization*, Phys. Rev. Lett. **115**, 220401 (2015), doi:10.1103/PhysRevLett.115.220401.

[60] A. Khodja, R. Steinigeweg and J. Gemmer, *Relevance of the eigenstate thermalization hypothesis for thermal relaxation*, Phys. Rev. E **91**, 012120 (2015), doi:10.1103/PhysRevE.91.012120.

[61] V. B. Bulchandani, D. A. Huse and S. Gopalakrishnan, *Onset of many-body quantum chaos due to breaking integrability*, Phys. Rev. B **105**, 214308 (2022), doi:10.1103/PhysRevB.105.214308.

[62] H. Spohn and J. L. Lebowitz, *Irreversible thermodynamics for quantum systems weakly coupled to thermal reservoirs*, Advances in Chemical Physics pp. 109–142 (1978), doi:https://doi.org/10.1002/9780470142578.ch2.

[63] R. Dümcke and H. Spohn, *The proper form of the generator in the weak coupling limit*, Zeitschrift für Physik B Condensed Matter **34**(4), 419 (1979), doi:10.1007/BF01325208.

[64] T. Mori and S. Miyashita, *Dynamics of the density matrix in contact with a thermal bath and the quantum master equation*, Journal of the Physical Society of Japan **77**(12), 124005 (2008), doi:10.1143/JPSJ.77.124005.

[65] A. Purkayastha, G. Guarnieri, M. T. Mitchison, R. Filip and J. Goold, *Tunable phonon-induced steady-state coherence in a double-quantum-dot charge qubit*, npj Quantum Information **6**(1), 27 (2020), doi:10.1038/s41534-020-0256-6.

[66] C. Uchiyama, *Dynamics of a quantum interacting system: Extended global approach beyond the born-markov and secular approximations*, Phys. Rev. A **108**, 042212 (2023), doi:10.1103/PhysRevA.108.042212.

[67] M. Łobejko, M. Winczewski, G. Suárez, R. Alicki and M. Horodecki, *Corrections to the hamiltonian induced by finite-strength coupling to the environment*, Phys. Rev. E **110**, 014144 (2024), doi:10.1103/PhysRevE.110.014144.

[68] R. Balian, *From Microphysics to Macrophysics*, Springer-Verlag Berlin, Heidelberg (2007).

[69] C. Bartsch and J. Gemmer, *Dynamical typicality of quantum expectation values*, Phys. Rev. Lett. **102**, 110403 (2009), doi:10.1103/PhysRevLett.102.110403.

[70] P. Reimann, *Dynamical typicality of isolated many-body quantum systems*, Phys. Rev. E **97**, 062129 (2018), doi:10.1103/PhysRevE.97.062129.

[71] H. Tal-Ezer and R. Kosloff, *An accurate and efficient scheme for propagating the time dependent Schrödinger equation*, The Journal of Chemical Physics **81**(9), 3967 (1984), doi:10.1063/1.448136.

[72] R. Chen and H. Guo, *The chebyshev propagator for quantum systems*, Computer Physics Communications **119**(1), 19 (1999), doi:https://doi.org/10.1016/S0010-4655(98)00179-9.

[73] V. V. Dobrovitski and H. A. De Raedt, *Efficient scheme for numerical simulations of the spin-bath decoherence*, Phys. Rev. E **67**, 056702 (2003), doi:10.1103/PhysRevE.67.056702.

[74] H. Fehske, J. Schleede, G. Schubert, G. Wellein, V. S. Filinov and A. R. Bishop, *Numerical approaches to time evolution of complex quantum systems*, Physics Letters A **373**(25), 2182 (2009), doi:https://doi.org/10.1016/j.physleta.2009.04.022.

[75] E. H. Lieb and D. W. Robinson, *The finite group velocity of quantum spin systems*, Communications in Mathematical Physics **28**(3), 251 (1972), doi:10.1007/BF01645779.

[76] M. P. Woods, M. Cramer and M. B. Plenio, *Simulating bosonic baths with error bars*, Phys. Rev. Lett. **115**, 130401 (2015), doi:10.1103/PhysRevLett.115.130401.

[77] M. P. Woods and M. B. Plenio, *Dynamical error bounds for continuum discretisation via gauss quadrature rules—a lieb-robinson bound approach*, Journal of Mathematical Physics **57**(2), 022105 (2016), doi:10.1063/1.4940436.

[78] L. F. Santos, *Integrability of a disordered heisenberg spin-1/2 chain*, Journal of Physics A: Mathematical and General **37**(17), 4723 (2004), doi:10.1088/0305-4470/37/17/004.

[79] M. Brenes, E. Mascarenhas, M. Rigol and J. Goold, *High-temperature coherent transport in the xxz chain in the presence of an impurity*, Phys. Rev. B **98**, 235128 (2018), doi:10.1103/PhysRevB.98.235128.

[80] M. Brenes, J. Goold and M. Rigol, *Low-frequency behavior of off-diagonal matrix elements in the integrable xxz chain and in a locally perturbed quantum-chaotic xxz chain*, Phys. Rev. B **102**, 075127 (2020), doi:10.1103/PhysRevB.102.075127.

[81] L. F. Santos, F. Pérez-Bernal and E. J. Torres-Herrera, *Speck of chaos*, Phys. Rev. Res. **2**, 043034 (2020), doi:10.1103/PhysRevResearch.2.043034.

[82] P. Łydżba, M. Mierzejewski, M. Rigol and L. Vidmar, *Generalized thermalization in quantum-chaotic quadratic hamiltonians*, Phys. Rev. Lett. **131**, 060401 (2023), doi:10.1103/PhysRevLett.131.060401.

[83] P. Tokarczyk, L. Vidmar and P. Łydżba, *Single-quasiparticle eigenstate thermalization*, Phys. Rev. E **109**, 024102 (2024), doi:10.1103/PhysRevE.109.024102.

[84] M. Gluza, J. Eisert and T. Farrelly, *Equilibration towards generalized Gibbs ensembles in non-interacting theories*, SciPost Phys. **7**, 038 (2019), doi:10.21468/SciPostPhys.7.3.038.

[85] C. Murthy and M. Srednicki, *Relaxation to gaussian and generalized gibbs states in systems of particles with quadratic hamiltonians*, Phys. Rev. E **100**, 012146 (2019), doi:10.1103/PhysRevE.100.012146.

[86] J. Cotler, N. Hunter-Jones, J. Liu and B. Yoshida, *Chaos, complexity, and random matrices*, Journal of High Energy Physics **2017**(11), 48 (2017), doi:10.1007/JHEP11(2017)048.

[87] H. Gharibyan, M. Hanada, S. H. Shenker and M. Tezuka, *Onset of random matrix behavior in scrambling systems*, Journal of High Energy Physics **2018**(7), 124 (2018), doi:10.1007/JHEP07(2018)124.

[88] X. Chen and A. W. W. Ludwig, *Universal spectral correlations in the chaotic wave function and the development of quantum chaos*, Phys. Rev. B **98**, 064309 (2018), doi:10.1103/PhysRevB.98.064309.

[89] J. Liu, *Spectral form factors and late time quantum chaos*, Phys. Rev. D **98**, 086026 (2018), doi:10.1103/PhysRevD.98.086026.

[90] P. Kos, M. Ljubotina and T. c. v. Prosen, *Many-body quantum chaos: Analytic connection to random matrix theory*, Phys. Rev. X **8**, 021062 (2018), doi:10.1103/PhysRevX.8.021062.

[91] E. J. Torres-Herrera, A. M. García-García and L. F. Santos, *Generic dynamical features of quenched interacting quantum systems: Survival probability, density imbalance, and out-of-time-ordered correlator*, Phys. Rev. B **97**, 060303 (2018), doi:10.1103/PhysRevB.97.060303.

[92] M. Schiulaz, E. J. Torres-Herrera and L. F. Santos, *Thouless and relaxation time scales in many-body quantum systems*, Phys. Rev. B **99**, 174313 (2019), doi:10.1103/PhysRevB.99.174313.

[93] S. Lerma-Hernández, D. Villaseñor, M. A. Bastarrachea-Magnani, E. J. Torres-Herrera, L. F. Santos and J. G. Hirsch, *Dynamical signatures of quantum chaos and relaxation time scales in a spin-boson system*, Phys. Rev. E **100**, 012218 (2019), doi:10.1103/PhysRevE.100.012218.

[94] P. Sierant, D. Delande and J. Zakrzewski, *Thouless time analysis of anderson and many-body localization transitions*, Phys. Rev. Lett. **124**, 186601 (2020), doi:10.1103/PhysRevLett.124.186601.

[95] A. Prakash, J. H. Pixley and M. Kulkarni, *Universal spectral form factor for many-body localization*, Phys. Rev. Res. **3**, L012019 (2021), doi:10.1103/PhysRevResearch.3.L012019.

[96] D. Basilewitsch, S.-D. Börner, C. Berke, A. Altland, S. Trebst and C. P. Koch, *Chaotic fluctuations in a universal set of transmon qubit gates* (2024), `2311.14592`.